④

**AD-A222 609**

## FINAL REPORT

# VIKING DATA ANALYSIS

DTIC
ELECTE
JUN 0 8 1990
S D

Office of Naval Research

Contract N00014-86-C-0159

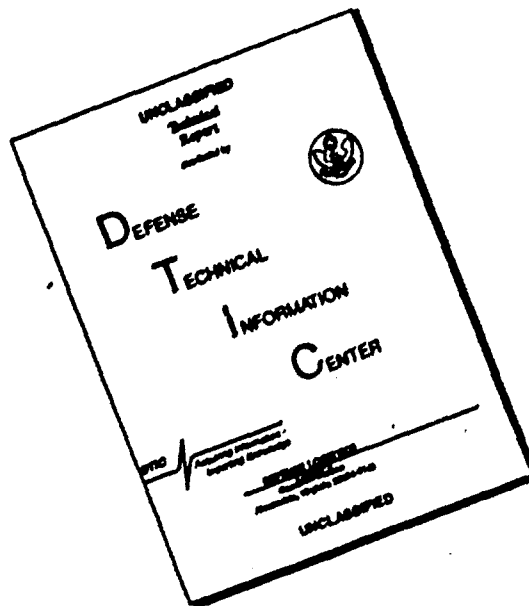Lockheed Space Sciences Laboratory

May 25, 1990

90 06 08 008

# DISCLAIMER NOTICE

THIS DOCUMENT IS BEST QUALITY AVAILABLE. THE COPY FURNISHED TO DTIC CONTAINED A SIGNIFICANT NUMBER OF PAGES WHICH DO NOT REPRODUCE LEGIBLY.

# REPORT DOCUMENTATION PAGE

Form Approved
OMB No. 0704-0188

| 1a. REPORT SECURITY CLASSIFICATION | 1b. RESTRICTIVE MARKINGS |
|---|---|
| Unclassified | |

| 2a. SECURITY CLASSIFICATION AUTHORITY | 3. DISTRIBUTION/AVAILABILITY OF REPORT |
|---|---|
| | Distribution unlimited. Cleared for |
| 2b. DECLASSIFICATION/DOWNGRADING SCHEDULE | public release and sale. |

| 4. PERFORMING ORGANIZATION REPORT NUMBER(S) | 5. MONITORING ORGANIZATION REPORT NUMBER(S) |
|---|---|
| | |

| 6a. NAME OF PERFORMING ORGANIZATION | 6b. OFFICE SYMBOL (If applicable) | 7a. NAME OF MONITORING ORGANIZATION |
|---|---|---|
| Lockheed Missiles and Space Company | | Office of Naval Research Code 1114 SP |

| 6c. ADDRESS (City, State, and ZIP Code) | 7b. ADDRESS (City, State, and ZIP Code) |
|---|---|
| Dept. 91-20, Building 255 3251 Hanover Street Palo Alto, CA 94304 | 800 North Quincy Street Arlington, VA 22217 |

| 8a. NAME OF FUNDING/SPONSORING ORGANIZATION | 8b. OFFICE SYMBOL (If applicable) | 9. PROCUREMENT INSTRUMENT IDENTIFICATION NUMBER |
|---|---|---|
| Office of Naval Research | Code 1114 SP | Contract No. N00014-86-C-0159 |

| 8c. ADDRESS (City, State, and ZIP Code) | 10. SOURCE OF FUNDING NUMBERS | | | |
|---|---|---|---|---|
| 800 North Quincy Street Arlington, VA 22217 | PROGRAM ELEMENT NO. 61153N | PROJECT NO. 4143 | TASK NO 4143104 | WORK UNIT ACCESSION NO. |

11. TITLE (Include Security Classification)

Viking Data Analysis

12. PERSONAL AUTHOR(S)  J.M. Quinn

| 13a. TYPE OF REPORT | 13b. TIME COVERED | 14. DATE OF REPORT (Year, Month, Day) | 15. PAGE COUNT |
|---|---|---|---|
| Final Technical | FROM 8/86 TO 3/90 | 90/05/25 | |

16. SUPPLEMENTARY NOTATION

| 17. COSATI CODES | | | 18. SUBJECT TERMS (Continue on reverse if necessary and identify by block number) |
|---|---|---|---|
| FIELD | GROUP | SUB-GROUP | Viking satellite, auroral ion acceleration, auroral |
| 20 | 09 | | morphology, ionosphere/magnetosphere coupling |
| 04 | 01 | | |

19. ABSTRACT (Continue on reverse if necessary and identify by block number)

The polar orbiting Swedish research satellite, Viking, obtained extensive data on auroral zone phenomena. Data from the Viking Hot Plasma Experiment have been analyzed to investigate auroral acceleration and the transport of plasma between the ionosphere and magnetosphere. A detailed statistical study was made of the relative location of ionospheric ion acceleration with respect to various magnetospheric plasma boundary signatures. The results indicate that the ion acceleration occupies a much wider latitudinal extent of the auroral zone than is expected by many current models; and that the regions of ion acceleration are ordered by, and move with, several magnetospheric plasma boundaries. Multi-spacecraft analyses of transverse ion acceleration by broadband low-frequency waves have been performed and indicate that this mechanism is an important factor in transporting plasma into the magnetosphere.

| 20. DISTRIBUTION/AVAILABILITY OF ABSTRACT | 21. ABSTRACT SECURITY CLASSIFICATION |
|---|---|
| ☐ UNCLASSIFIED/UNLIMITED  ☒ SAME AS RPT  ☐ DTIC USERS | Unclassified |

| 22a. NAME OF RESPONSIBLE INDIVIDUAL | 22b. TELEPHONE (Include Area Code) | 22c. OFFICE SYMBOL |
|---|---|---|
| R. Gracen Joiner | 202-696-4216 | ONR 1114 SP |

DD Form 1473, JUN 86          Previous editions are obsolete.          SECURITY CLASSIFICATION OF THIS PAGE

# FINAL REPORT

# VIKING DATA ANALYSIS

## Contract N00014-86-C-0159

## May 25, 1990

J.M. Quinn
Lockheed Space Sciences Laboratory
415-424-3289

# TABLE OF CONTENTS

# ABSTRACT

The polar orbiting Swedish research satellite, Viking, obtained extensive data on auroral zone phenomena. Data from the Viking Hot Plasma Experiment have been analyzed to investigate auroral acceleration and the transport of plasma between the ionosphere and magnetosphere. A detailed statistical study was made of the relative location of ionospheric ion acceleration with respect to various magnetospheric plasma boundary signatures. The results indicate that the ion acceleration occupies a much wider latitudinal extent of the auroral zone than is expected by many current models; and that the regions of ion acceleration are ordered by, and move with, several magnetospheric plasma boundaries. Multi-spacecraft analyses of transverse ion acceleration by broadband low-frequency waves have been performed and indicate that this mechanism is an important factor in transporting plasma into the magnetosphere.

# BACKGROUND

On February 21, 1986 the Swedish research satellite, Viking, was launched to study ionospheric and magnetospheric processes at high latitudes. A summary of the Viking scientific objectives and its instrumentation is given in Reference 1, which is attached as Appendix D. Both the polar elliptical orbit, with an apogee of approximately 15,000 km., and the instrument complement were particularly suited to in situ studies of the complex physical processes associated with the auroral acceleration region. Of particular interest is Viking's coverage of the important altitude region above the 8,000 km. limit of the pioneering measurements made by UNR instruments on S3-3.

During the normal Viking operational period, which ended in December 1986, several "campaigns" addressed specific scientific problems. During each campaign particular instrument modes were selected under real time control of the investigators, in coordination with operations by ground based instruments and other satellites, in order to gain detailed information on particular phenomena and in response to questions raised by earlier measurements.

The Viking instrument complement was very complete, with measurements of electric and magnetic fields; plasma density, composition, and distribution functions; electric and magnetic waves; and ultraviolet images of the aurorae. The five instrument groups, designated V1 - V5, are summarized in Table 1.

The Lockheed Palo Alto Research Laboratory (LPARL) received partial support from ONR to build the onboard data processing unit for the "V3" group of instruments which are dedicated to the measurements of hot plasmas. The measurement capabilities of the V3 instrument group are summarized in Table 2.

As Co-Investigators on the V3 team, LPARL has collaborated extensively with the Swedish Institute of Space Physics (in Swedish: Institutet for rymdfysik -- "IRF") in the exchange of data and the analysis of several topics of interest. We have also collaborated with several other groups whose data from other instruments, both on Viking and other satellites, provide important complementary information to the V3 results.

In August of 1986, LPARL received an ONR contract (N00014-86-C-0159) to perform preliminary analysis of data from the Viking hot plasma

2

TABLE 1

## Viking Experiment Summary

V1 Electric Field Vector Experiment:
Quasistatic electric field with three component vector measurements,
including swept E-field probes for plasma density measurements.
L. Block, Principal Investigator

V2 Magnetic Field Experiment:
Precision measurements of the vector magnetic field for studies of the
field aligned electric currents and determination of particle pitch angles.
T. A. Potemra, Principal Investigator

V3 Hot Plasma Experiments:
Low energy particle spectrometers, energetic ion composition spectrometers
and high energy particle detectors to provide measurements of the plasma
distribution functions and ion composition.
R. Lundin, Principal Investigator

V4 Wave Experiments:
Low and high frequency wave experiments, $\Delta n/n$ probes and a resonance
experiment to determine plasma instabilities, wave generations,
wave/particle interactions and plasma densities.
High frequency part - A. Bahnsen, Principal Investigator
Low frequency part -  B. Holback, Principal Investigator

V5 Ultraviolet Auroral Imager:
Measurement of the distribution of auroral emissions in ultraviolet light.
C. D. Anger, Principal Investigator

TABLE 2

## Hot Plasma Experiment

| Unit | Measurement Objectives |
|------|------------------------|

V3-1    Energy- and pitch angle distribution of <u>electrons</u> with a high
        spectral resolution ($\Delta E/E \sim 0.05$). From $\sim 10$ eV to $\sim 40$ keV in up to
        128 energy levels.

V3-2    Energy- pitch angle distribution of <u>electrons</u> with a high angular
        resolution ($\Delta \alpha \leq 2^\circ$) from $\sim 0.1$ keV to $\sim 300$ keV in 16 energy levels.

V3-3    Energy- pitch angle distribution of energetic <u>positive ions</u>. From
        $\sim 40$ eV to $\sim 40$ keV in up to 64 energy levels ($\Delta E/E \leq 0.08$, $\Delta \alpha \leq 6^\circ$).

V3-4    3-Dimensional distribution function measurements of <u>positive ions</u>
        from $\sim 1$ eV to 10 keV in up to 32 energy levels.

V3-5    Measurements of the energy and pitch angle distribution of $\underline{H^+}$, $He^{++}$,
        $\underline{He^+}$ and $\underline{O^+}$ from $\sim 50$ eV/q to 20 keV/q in up to 16 energy levels ($\Delta \alpha$
        $\sim 6^\circ$-$12^\circ$).

V3-6    Detailed <u>ion composition</u> measurements from $\sim 1$ eV/q to $\sim 70$ keV/q in up
        to 32 energy levels ($M/\Delta M \sim 1$-7 for energies less than $\sim 20$ keV/q).

V3-7    Detailed composition, energy- pitch angle distribution measurements
        of <u>energetic positive ions</u> from 10 keV/nucleon to 10 MeV/nucleon.

instruments and to evaluate specific events and phenomena as candidates for more detailed investigation. Based on a proposal dated January 15, 1987, this contract was extended to allow detailed investigation of the V3 data. The results of this investigation are described in the following section.

# PROGRESS

## DATA BASE AND ANALYSIS TOOLS

The main operational period of Viking, during which science instruments were operated essentially continuously, extended from launch in February, 1986 until December, 1986. A broad array of tools have been developed, both at Lockheed and at the Swedish IRF, for the display and analysis of these data.
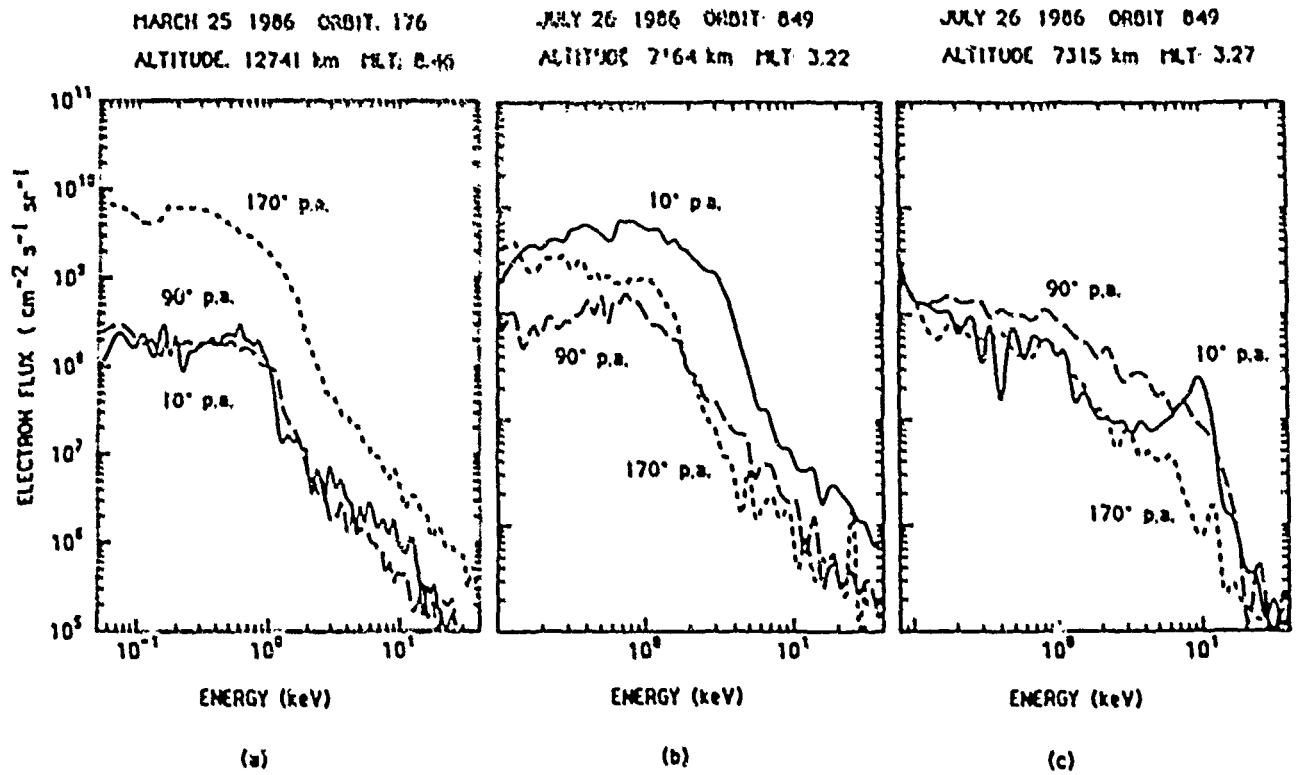
In order to survey the data and to select events for more detailed investigation, IRF developed a set of microfiche for over 1500 orbits. There are several types of microfiche formats, with 10-20 frames for each orbit. A "summary" display presents selected key data from all Viking instruments, in addition to grayscale output from the imager. A separate set of microfiche displays very complete V3 data in the form of color spectrograms for both ion/electron (non-mass resolved) as well as ion composition. These V3 spectrograms provide very good time and energy resolution, enabling immediate identification of pitch angle structure, ion and electron population boundaries, and various convection signatures.

A quantitative analysis of the V3 data may be performed using data from the "Data Summary Files" that were provided by IRF on magnetic tapes. A description of the contents of these files is included as Appendix C. We developed under this contract several software modules to extract data from these tapes and to process it into several formats. In addition to making various detailed line plots, for instance flux versus energy, the tape handling software also added information from each tape processed to a database that serves as an index to the data contained on the tape. The Swedish IRF contributed supplementary data display formats for various specialized analyses of plasma characteristics.

Figure 1 is an example of electron displays for orbits 176 and 849. This type of plot is extremely useful for analyzing the details of the electron pitch angle structure. In particular, the plots provide a very convenient means for comparing the pitch angle character in different energy ranges.

Coordinated studies between Viking and other satellites frequently require knowledge of two or more satellites' orbital tracks and the relative timing of their passage through particular regions. The most common requirements are to assess the conjugacy of satellites along a magnetic field line, or to clarify the timing of their passages through particular local time

# Examples of Electron Flux Spectra



(a) MARCH 25 1986  ORBIT  176
ALTITUDE  12741 km  MLT  8.46

(b) JULY 26 1986  ORBIT  849
ALTITUDE  7164 km  MLT  3.22

(c) JULY 26 1986  ORBIT  849
ALTITUDE  7315 km  MLT  3.27

VIKING-V3  ELECTRONS
DATE: 860325
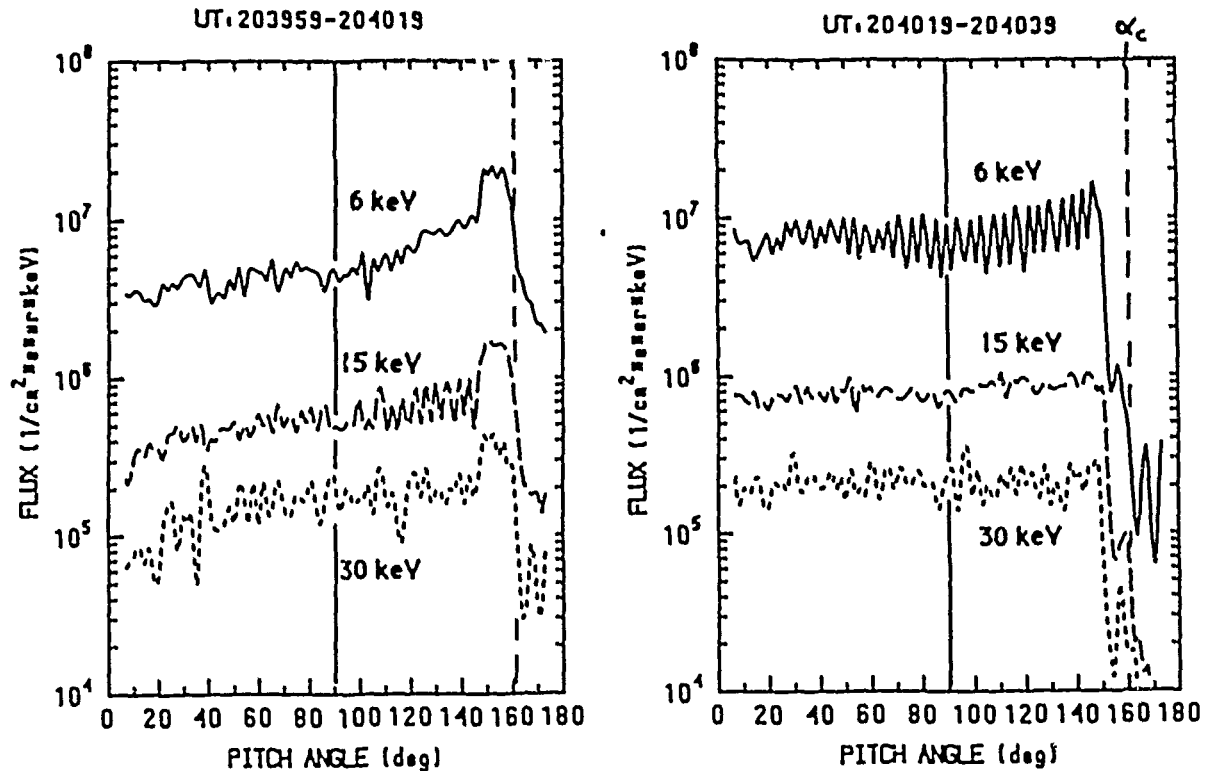ALT: 7074. km  INVL: 75.3
MLT: 20.34 ORBIT: 176

Figure 1

7

or magnetic latitude regions. The principal satellites used for comparison with Viking are SCATHA, to provide equatorial data during a Viking cut through the auroral zone, and Dynamics Explorer, to give comparative auroral zone data from a different altitude or the conjugate hemisphere.

In order to evaluate Viking's orbits with respect to other satellites we have developed software to plot the orbital tracks. An example is shown in Figure 2. The figure displays 20 minute segments of the Viking and Dynamics Explorer orbits as they pass through high latitude field lines in opposite hemispheres. The top two panels show the orbits as viewed from 18:00 and 12:00 local time. Magnetic field lines intersecting the orbits are traced at 10 minute intervals. The lower left panel displays the orbital paths in local time and invariant latitude. The case shown is for a peri d that was investigated by the ninth Coordinated Data Analysis Workshop (CDAW-9). A discussion of the CDAW-9 analysis is presented in a later section.

## LOCATIONS OF ION ACCELERATION WITH RESPECT TO PLASMA BOUNDARIES

In many ways the Viking program represents a natural follow-on to the extraordinarily rich S3-3 mission. Among the many key results of S3-3 was the identification of auroral ion acceleration processes extending over a very sizable range of latitude/local time space. It was also clear from S3-3 that these processes were operative throughout a surprisingly large altitude region, to well above the 8,000 km S3-3 apogee. The Viking instrumentation suite and orbit were chosen to address many of the questions that were raised by the S3-3 results. In particular, the orbit significantly extends the altitude coverage and provides apogee precession through auroral latitudes early in the mission.

Figure 3 illustrates the variation throughout the main Viking operational period of two of the orbital parameters that serve as selection criteria for studies of auroral processes. The top portion of the figure shows magnetic local time of Viking equator crossings, thus indicating the local time orientation of the orbit. The bottom portion of the figure displays the latitude of apogee, which provides an indication of the altitude at which the auroral region is sampled at various periods. One can see from Figure 3 that within approximately the first hundred days of the mission, Viking's apogee moved through auroral latitudes while in the dawn local time region. As described below, this period provided an
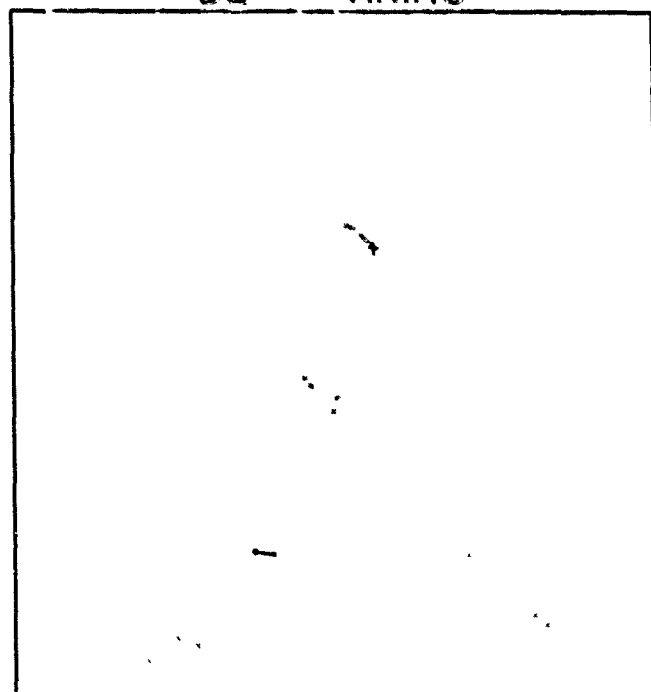
DE — VIKING

DE — VIKING

2   Hr: 18:00   Lat:   0.0   Alt:   10.0
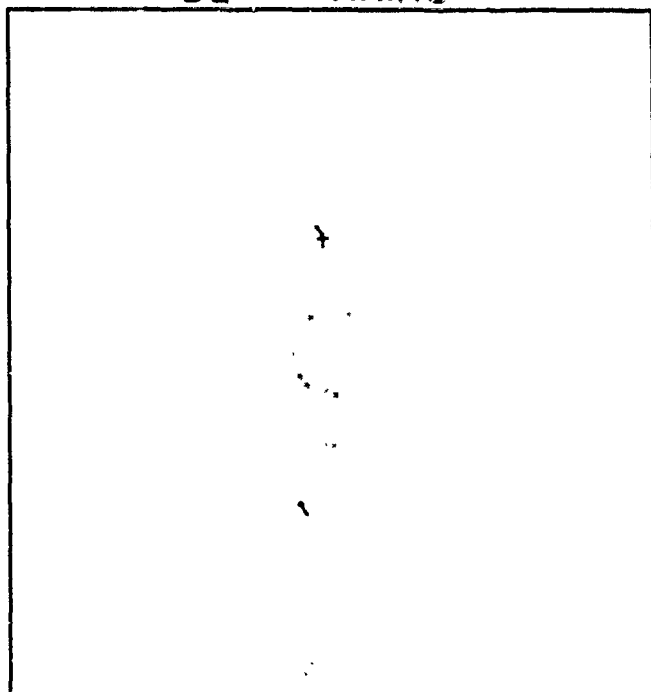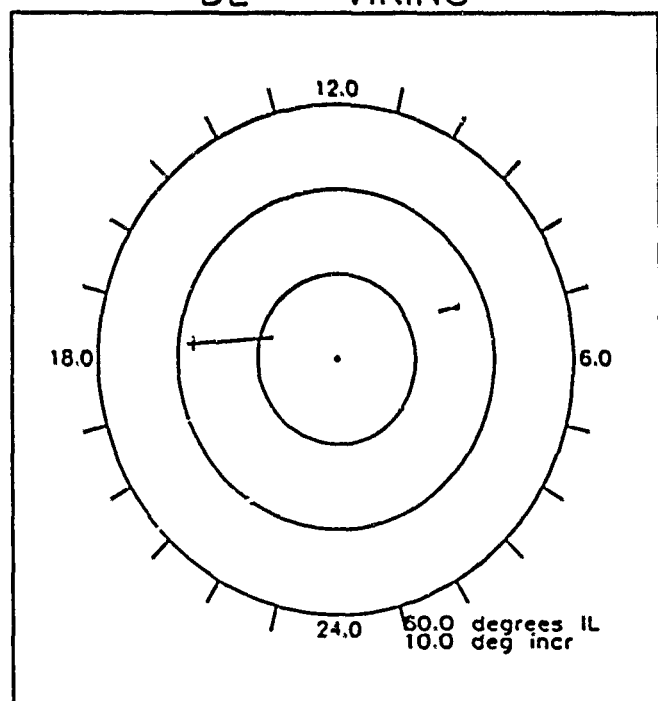
1   Hr: 12:00   Lat:   0.0   Alt:   10.0

DE — VIKING

| Color | Satellite | Start/Stop | | dT |
|---|---|---|---|---|
| ▨ | DE | · 1986 124 11:45 | | 0.10 |
| | | 1986 124 12:15 | | |
| ▨ | VIKING | + 1986 124 11:45 | | 0.10 |
| | | 1986 124 12:15 | | |

12.0

18.0

6.0

24.0   60.0 degrees IL
       10.0 deg incr

100.0   76.8   53.5   30.3   7.0
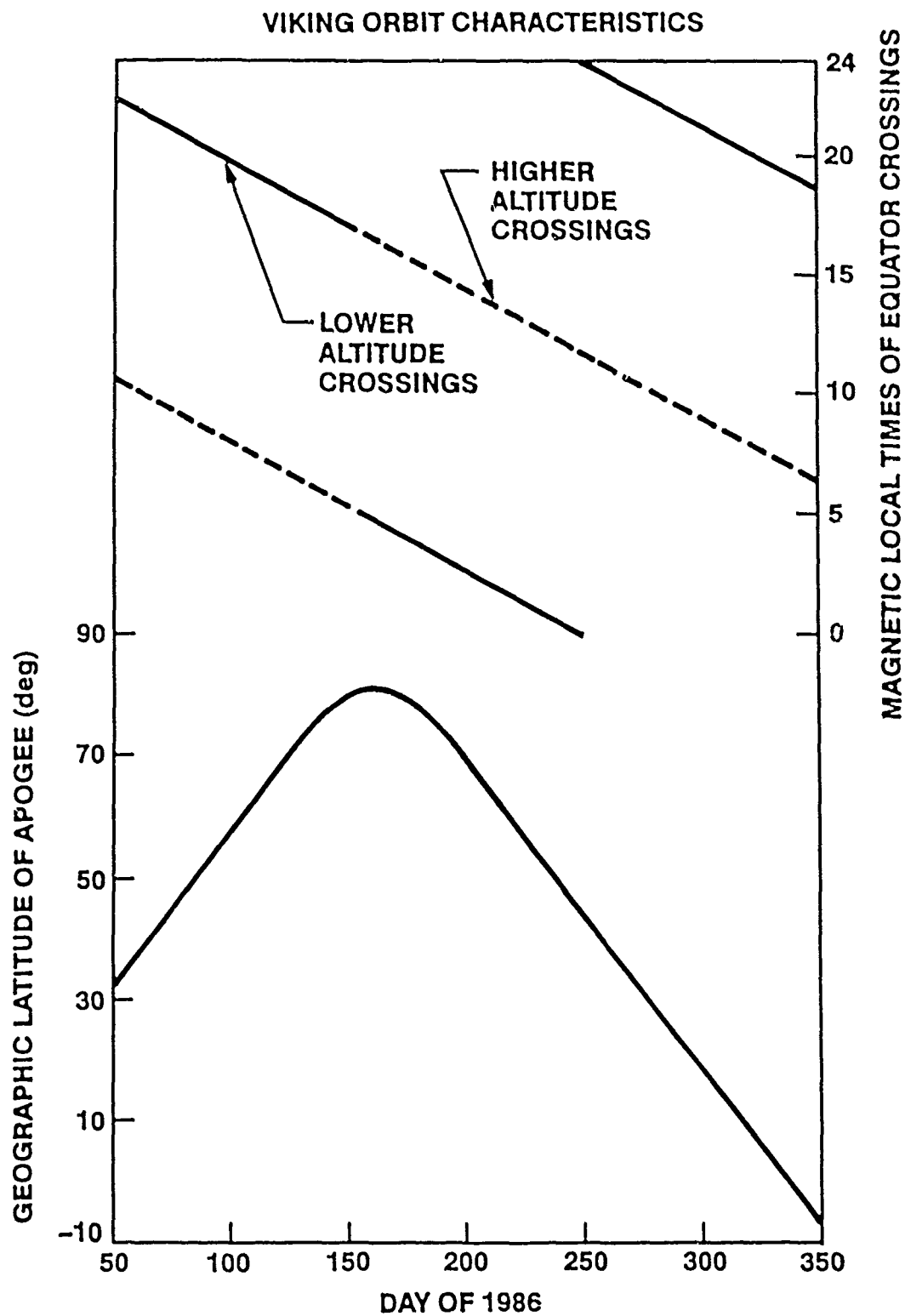2.0     3.3    4.5    5.8    7.0

Figure 2

9

Figure 3

10

excellent data set for an analysis of the location of auroral ion acceleration with respect to plasma boundaries.

Morphological studies on S3-3 and following missions have determined in some detail the statistical locations of auroral ion acceleration and the resulting outflow of ionospheric plasma into the magnetosphere. Equatorial satellites at geosynchronous orbit and higher altitudes have observed these ions as they become part of the trapped magnetospheric plasma populations, however there is a good deal of uncertainty about the equatorial distribution of ionospheric plasma injection. Workers with both equatorial and polar orbiting spacecraft have devoted considerable effort to identifying the plasma characteristics of various regions (e.g. plasma sheet, tail lobes, polar cap, auroral zone). However a mapping between the equatorial and polar data is exceedingly difficult. There is considerable controversy about the identification of various equatorial plasma populations with their counterparts observed at high latitudes from polar orbit. Thus it is quite difficult to make full use of the ionospheric outflow data in models of magnetospheric plasma transport.

In order to clarify the latitudinal/L-shell location of ionospheric outflow with respect to magnetospheric plasma populations we have performed a detailed study of 40 days of Viking data, representing some 89 cuts through the northern hemisphere auroral zone for which data are available. For each pass, we identified the latitudinal positions of all occurrences of upflowing ions, together with the positions of several types of plasma populations. In contrast to previous studies showing the statistical latitudinal positions of ion outflow, this database provides a means to evaluate directly the relative position of ion acceleration with respect to key plasma populations. This provides the opportunity to evaluate in a statistically meaningful fashion the locations of ion outflow as it maps into the magnetosphere. Previous analyses of this type have been limited to a few case studies.

The results of this study were reported to the scientific community in References 3 and 6. A copy of the manuscript for Reference 6 is attached as Appendix A. Some of the principal results of this study are the following:

**On the dawn side, upflowing ions typically occur over a 5 degree extent of invariant latitude.** This is in contrast to theories which predict auroral ion acceleration mechanisms to be limited to very narrow regions, for instance in association with discrete auroral

11

arcs. While some orbits do show only narrow regions of upflow (1 degree or less), others show a very wide latitudinal extent.

The dawn ion upflow is ordered by, and moves with, the poleward boundary of continuous, > 1keV, ions. The occurrence frequency distribution is centered on this boundary, and is approximately symmetric about it. The occurrence frequency distribution about the continuous ion boundary is much narrower than the raw latitudinal distribution, and is approximately the same width as the average typical latitudinal extent. Thus the continuous ion boundary is closely coupled with the upflowing ion location. The upflow is also well ordered, although not quite as well, by the poleward boundary of continuous electrons. The locations of the continuous ion boundaries and continuous electron boundaries are well correlated with each other. The continuous ion boundary is on average 1.5 degrees poleward of the continuous electron boundary.

The latitudinal width of ion upflow is well correlated with magnetic activity (Kp and Ae). The average width during quiet periods is 3.5 degrees, increasing to approximately 6 degrees during active times.

The results obtained on the dawn side from the Viking data are complementary and in general agreement with other investigations performed for the dusk region using S3-3 data (References 2 and 7). It is expected that these analyses of the locations of ion upflow with respect to plasma boundaries will provide an important key to the understanding of the mapping and plasma transport between the auroral zone and the outer magnetosphere.

## ION HEATING BY LOW FREQUENCY WAVES AND CDAW-9 SUBSTORM EVENT

Beginning with S3-3, data from polar orbiting satellites have indicated that upflowing ions frequently contain strong signatures of transverse energization. That is, in addition to the magnetic field aligned distributions that result from acceleration by parallel electric fields, the ion pitch angle distributions are often peaked at some angle other than the field aligned direction. These distributions may be simple "conics" in which all energies are peaked at the same pitch angle, indicating a transverse acceleration at some relatively localized altitude below the spacecraft; or they may include

more complex energy-angle structure such as results from combinations of parallel and transverse energization over a range of altitudes.

In recent years there has been considerable interest in understanding the transverse energization of ions through their interaction with low frequency waves. The Viking data provide an excellent opportunity to study this phenomenon in coordinated investigations with simultaneous data from other spacecraft. In particular, the ninth Coordinated Data Analysis Workshop (CDAW9) provided an opportunity to investigate wave driven ion heating at the time of substorm onset.

The Coordinated Data Analysis Workshop (CDAW) is an ongoing program to gather data and investigators from a large number of space- and ground-based instrument groups to analyze one or more selected events of interest in great detail. Th Focus is often on substorm initiation and dynamics. CDAW9-D addressed a substorm that occurred on May 4, 1986, beginning as Viking and Dynamics Explorer (DE) were traversing high latitude field lines near the dawn-dusk plane. Viking was in the northern hemisphere near dawn, while DE was in the southern hemisphere near dusk (see Figure 2). Shortly following the substorm onset, identified in the Viking images at 11:53 UT, both Viking and DE observed "ion bowl" type pitch angle distributions. Intense electric and magnetic field turbulence was observed below the Oxygen gyrofrequency by both satellites. The data would appear to indicate that global wave activity associated with the substorm onset is responsible for the creation of the transversely energized ion populations seen at both spacecraft. However, the time between the substorm onset and the observation of the energized ion populations (4 minutes) is too short for any of the standard substorm models. As the SCATHA satellite also observed magnetometer signatures from a position sunward of Viking and DE, it may be that another interpretation is required. The results of this study were presented to the scientific community (Reference 4) and are the basis of an ongoing dialog among many researchers associated with CDAW9.

In order to confirm the viability of low-frequency broadband. waves as a heating mechanism for ion conic distributions, we have collaborated with a number of investigators in comparing observed conic distributions with theoretical predictions. A detailed analysis of one conic observed during a cusp/cleft crossing has been performed and reported in Reference 5. Observed cool $O^+$ distributions and observed wave intensities were used as input to a Monte Carlo simulation. The hot $O^+$ distributions resulting from this simulation are in good agreement with the corresponding

observed distributions. We believe that these and other collaborative investigations show that resonant heating by broadband low-frequency waves is an important mechanism in the outflow of ionospheric ions into the magnetosphere.

# REFERENCES

(1) "The Viking Program", The Viking Science Team, Trans. Amer. Geophys. Union, Vol 67, No. 42, 793, 1986.

(2) "Spatial Relationship between Ion Acceleration Regions and Plasma Sheet Boundaries", J.M. Quinn, A.G. Ghielmetti, E.G. Shelley, Proceedings of the XIX General Assembly of the International Union of Geodesy and Geophysics, V.2, 584, 1987.

(3) "The Latitudinal Location and Extent of Ion Acceleration Regions in the Post-Midnight Sector", J.M. Quinn, A.G. Ghielmetti, R.N. Lundin, Trans. Amer. Geophys. Union, Vol. 69, No. 44, 1396, 1988.

(4) "Coordinated Observations of Low Frequency Wave Turbulence and Ion Energization during a Magnetospheric Substorm", W.K. Peterson, H.L. Collin, G.B. Crew, M. Andre, J. Woch, P-A. Lindqvist, M.J. Engebretson, A.M. Persoon, R.E. Erlandson, Trans. Am. Geophys. Union, Vol 70, No. 43, 1282, 1989.

(5) "Ion Heating by Broadband Low-Frequency Waves in the Cusp/Cleft", M. Andre, G.B. Crew, W.K. Peterson, A.M. Persoon, C.J. Pollock, M.J. Engebretson, Proceedings of the European Geophysical Society, Spring Meeting, 1990.

(6) "Extent and Relative Locations of Auroral Acceleration Regions I: Post-Midnight Sector", J.M. Quinn, A.G. Ghielmetti, R.N. Lundin, to be submitted J. Geophys. Res., 1990.

(7) "Extent and Relative Locations of Auroral Acceleration Regions II: Pre-Midnight Sector", A.G. Ghielmetti, J.M. Quinn, R.N. Lundin, to be submitted J. Geophys. Res., 1990.

# APPENDIX A

"The Extent and Relative Locations of Auroral
Acceleration Regions I:   Post-Midnight Sector"

# EXTENT AND RELATIVE LOCATIONS OF AURORAL ACCELERATION REGIONS I: POST-MIDNIGHT SECTOR

J.M. Quinn, A.G. Ghielmetti (Lockheed Space Sciences Laboratory)

R.N. Lundin (Swedish Institute of Space Physics)

## ABSTRACT

Ion data from the Viking satellite are used to identify auroral acceleration structures in the post-midnight local time sector. The locations of these ion acceleration regions are compared to four particle boundaries inferred from the isotropic electron and ion fluxes. In the post-midnight region, acceleration structures are often observed to occur over a substantial width in latitude ($5^\circ$) and are statistically centered about a boundary representing the poleward edge of contiguous energetic ion fluxes. The position of this boundary with respect to other particle boundaries and as a function of magnetic activity are also examined.

# 1. INTRODUCTION

In this paper we consider the latitudinal location of auroral region ion acceleration relative to various signatures of the surrounding plasma populations. Previous statistical studies have determined the absolute latitudinal positions of energetic ion outflow as a function of local time. Similar statistical investigations have been performed for most other key auroral zone phenomena such as electron precipitation, electric field structure, currents, and auroral emissions. However, only a limited number of detailed case studies have explored the "instantaneous" *relative* location of upflowing ionospheric ions in the context of other auroral features. Thus, although we know statistically the independent latitudinal positions of many auroral zone plasma features, there is not a sound basis upon which to draw conclusions regarding their "typical" latitudinal relationship to auroral ion acceleration. In this paper we hope to provide a bridge between the statistical and the detailed case studies by examining the "instantaneous" relative locations of ion outflow to other plasma signatures over a fairly large number (89) of polar orbital cuts by the Viking satellite.

The identification of auroral zone ion acceleration has generally relied upon two techniques: the direct measurement of upflowing ions, observed above or within the acceleration region, and the inference of upward directed parallel electric fields above the spacecraft from electron pitch angle signatures (e.g. Cladis and Sharp, 1979; Sharp et al. 1979). The statistical morphology of the directly measured outflowing ions has been extensively characterized using data from S3-3 (Ghielmetti et al., 1978; Gorney et al., 1981; Sharp et al., 1983) and DE (Yau et al., 1984; Yau et al., 1985; Collin et al., 1988). The average local time and invariant latitude distributions presented in these studies are generally consistent with the auroral oval, although there is significant variation with the upflowing ions' energy and pitch angle character (beam vs. conic). While these studies show that the absolute latitudinal range within which ion acceleration is observed is quite large (> 10 degrees), examples from individual orbits show the instantaneous latitudinal extend to be highly variable, from less than 1 degree to greater than 5 degrees (e.g. Ghielmetti et al., 1978).

Case studies addressing the latitudinal location of auroral ion acceleration with respect to the high latitude signatures of various plasma populations have provided a good deal of insight into the magnetospheric context of the ion acceleration process (Winningham et al., 1975; Heelis et al., 1980; Mizera et al., 1981). However, the identification of latitudinal

structures observed by polar orbiting satellites with features that have been identified in the equatorial region is made difficult by uncertainties in the magnetic field mapping and by differences in the measurements imposed by orbital constraints. An excellent review by Feldstein and Galperin summarizes the plethora of (sometimes conflicting) terminology that has been applied to plasma sheet morphology and highlights the difficulties in identifying a self consistent picture.

In this paper we present the results of a statistical study of the latitudinal location of ion upflow with respect to the signatures of the ambient plasma population, as observed by the Viking in apogee passes through the dawn-side auroral zone. A companion paper will present complementary dusk-side results from S3-3 (Ghielmetti et al., 1990)

## 2. DATA SELECTION AND ANALYSIS

The data used in this study were acquired by the V3 hot plasma instrument complement aboard the polar orbiting Viking spacecraft. This satellite was launched into a highly eccentric orbit with a perigee of 817 km, apogee of ~13500 km , and inclination of 98 degrees in early 1986. The spacecraft was spinning in a near cartwheel mode at 3 rpm and hence full pitch angle distributions were obtained every 20 seconds. The instrument included a set of three electron spectrometers orientated at 70, 90 and 110 degrees that covered the energy range from 10 eV to 40 keV in less than 0.6 sec. Two ion spectrometers mounted at 90 degrees relative to the spin axis measured the total ion fluxes in the range from 40 eV to 40 KeV with the same temporal resolution. More complete descriptions of the instrumentation are given in Sandahl et al (1985).

The data selected for this investigation were acquired between April 24 and June 2 1986. During this 40 day period the satellite orbit crossed the dawn side auroral oval at high altitudes (> 11000 km), thus maximizing the probability for ion accelerations below the satellite (Ghielmetti et al., 1978, Gorney et al., 1981). For the present study, we required the absence of cusp like dispersion signatures in the ion fluxes. A total of 89 orbits that met the above criteria provided near uniform sampling of the local time region from ~06.00 to ~08.00 MLT, and latitudes from 65 to 80 degrees ILA (Figure 1). The period selected is characterized by generally low magnetic activity and is near the minimum of the solar cycle.

Ion and electron microfiche data in the form of color coded energy-time spectrograms were visually scanned for signatures of upward flowing

ions (UFI), and for presence of isotropic fluxes above a threshold level. For the purpose of the present study an UFI region required the existence of a pitch angle anisotropy with flux peaking in the upward direction on at least two consecutive spins for ion energies > 100 eV. Each contiguous region of ion upflow was characterized by its extent in latitude, the typical energy range of the UFI's, and the predominant pitch angle type (field aligned or conical).

In addition to identifying UFI regions within each orbit, we also defined several latitudinal boundaries for the ambient plasma. In the more equatorward high latitude region ( <~ 70 deg ILA ) the keV electron fluxes observed with Viking typically decreased gradually with decreasing latitude and did not exhibit a well defined flux discontinuity. Similarly, the fluxes of > 1 keV ions were typically seen down to the lowest latitudes inspected (< 65 deg) without any evidence of systematic discontinuities. As a result it is not meaningful to define an "inner boundary" based on some arbitrary flux level in the particle distributions. However, at higher latitudes both the electron and ion fluxes at energies > 1 keV typically exhibit one or several flux discontinuities that can be used to define a "poleward boundary". Although structured fluxes of lower energy (< 1 keV) electrons were often seen to extend even further poleward, only the energetic plasma boundaries were used for the present study.

To characterize latitudinally the location of the isotropic energetic plasma we therefore introduce the following "boundary" definitions

1.  Continuous Electron Boundary (CEB): The most poleward latitude at which >= 1 keV electron fluxes were observed continuously at lower latitudes (no gaps or flux dropouts at lower latitudes).

2.  Poleward Electron Boundary (PEB): The most poleward latitude at which >= 1 keV electron fluxes were observed. (By definition, PEB is >= the CEB).

3.  Continuous Ion Boundary (CIB): Same as CEB, but for ions.

4.  Poleward Ion Boundary (PIB): Same as PIB, but for ions.

In identifying the above boundaries a flux discontinuity was defined as a decrease in the energy flux below the sensitivity threshold of the instrument lasting for multiple (>= 2) satellite spins. Figure 2 schematically illustrates the boundary definitions together with typical features observed in the electron and ion fluxes.

To illustrate the ion end electron structures encountered we present in Figure 3 a sample energy-time spectrogram for a near dawn auroral zone pass. In this particular case the CEB was identified at 75.5 degrees ILA and the PEB at 80.3 degrees, while the ion boundaries were located at 76.4 degrees (CIB) and 80.0 degrees (PIB). Upward flowing ions with field aligned pitch angle distributions are seen to occur on every spin between about 17:22 and 17:32 hr UT. This contiguous region of ion upflow shows consistently field aligned distributions (beams) with energies from ~ 0.1 to 2 keV, while the flux intensities and energy distributions vary noticeably. In the present survey, the distinction between beams and conics, and the energy of UFI, are not utilized, although as described above they were included in the database.

# 3. RESULTS

Figure 4 provides an overview of the latitudinal locations of upflowing ions observed over the period of study, together with the simultaneously identified location for two of the particle boundaries. For each orbit, the invariant latitude range(s) over which upflowing accelerated ions were observed are indicated by vertical bars. In many of the orbits multiple, latitudinally distinct, regions of UFI were seen. As many as five separate regions of UFI were resolved during individual orbits, indicative of the significant amount of structure in the acceleration process. Out of the 89 orbits studied, only 4 contained no regions of UFI.

The polar boundary of continuous energetic ions (CIB), as defined in Section 2, is represented on Figure 4 as a solid line, drawn to connect the individual sampling points. The corresponding boundary for electrons (CEB) is indicated by shading at latitudes below the boundary. The ion boundary is seen to be generally poleward of the electron boundary, with the average displacement between the two of 1." degrees.

Several features of Figure 4 are immediately apparent. First, for individual passes, the identified regions of UFI extend over a latitudinal range of many degrees. Second, the UFI seem to follow the locations of the isotropic particle boundaries as they move in latitude. Finally, the two, independently determined, particle boundaries track each other fairly closely. A quantitative analysis supports each of these points, as will be shown below.

The occurrence frequency distribution in one degree invariant latitude bins is presented in Figure 5 for the UFI identified in this study . Both the latitudinal distribution and probability values are in general agreement with previous statistical studies of the latitudinal distribution of UFI (e.g. Gorney et al., 1981; Yau et al., 1984; Collin et al., 1988). Although differences in instrument energy coverage, altitude range of sampling, and phase of solar cycle make a quantitative comparison somewhat difficult, we can conclude that the distribution of UFI identified in this study are consistent with the previous results.

As with previous studies of UFI, the Viking data confirm that the acceleration processes that are responsible for ion outflow are active a large fraction of the time. Even a the raw distribution in invariant latitude shows probabilities greater than 60% in three of the 1 degree latitude bins.

Much more sharply peaked distributions are obtained when the UFI position is examined relative to the particle boundaries identified for each orbit. Figure 6 shows the UFI occurrence frequency in 1 degree latitudinal bins relative to the CIB. It is clear from comparison with Figure 5 that a significant degree of ordering is obtained by relating the UFI positions to the CIB. Clearly, it not surprising that such an ordering should be obtained with respect to this boundary, or with respect to any other feature that would b' expected to move with the overall enlargement and contraction of the auroral oval. Indeed latitudinal peaks that are nearly as sharp, but with offsets, are obtained when the UFI positions are measured with respect to the CEB.

The magnitudes of the 1 degree UFI probabilities represented in Figure 6 are quite impressive. The peak probability of 88% that is uncovered by comparison to the continuous ion boundary position is significantly higher than has been determined by previous studies of ion upflow, which have looked only at absolute latitude distributions and thus were subject to significant smearing by common latitudinal motion of auroral structures. It is worth noting, however, that even with the good ordering shown in Figure 6, there are still 5 1-degree bins with higher than 50% probability for observing UFI.

From inspection of Figure 4, one might suspect that the approximately 5° FWHM distribution with respect to the continuous ion boundary (Figure 6) results primarily from the intrinsic latitudinal width of the instantaneous UFI distribution. In order to verify this, we show in Figure 7 the occurrence frequency for the integrated latitudinal width of UFI from each orbit. This width represents only the sum of the individual UFI segments

from each orbit (not the difference between minimum and maximum latitudes at which UFI were observed). As anticipated, Figure 7 shows that the integrated regions of UFI most commonly occupy an "instantaneous" latitudinal extent of 4 to 5 degrees.

The isotropic particle boundaries defined in Section 2 were derived from independent observations. In order to examine whether a relationship exists between these boundaries we provide in Figure 8a a scatter plot of the latitude of the continuous ion- and the continuous electron boundaries (CIB and CEB) for all orbits within the data set. A linear regression analysis yields a correlation coefficient r = 0.86, with n=85, which is significant at < 0.01%. This good correlation suggests that the two boundaries move in concert. The CEB is, on average, offset in the equatorward direction from the CIB by 1.5° The correlations between the other isotropic boundaries are not as good but are nevertheless significant.

Further analysis shows that the isotropic particle boundaries move equatorward with increasing magnetic activity. Both the CIB and CEB are well correlated with $K_p$ and $A_E$. A particularly good correlation is observed for the CIB (Figure 8b) with r=-0.64 at < 0.01% significance. A weaker but significant correlation with magnetic activity is observed for the integrated latitudinal width of the UFI regions from each orbit (Figure 9).

## 4. DISCUSSION

The above observations suggest that the continuous isotropic particle boundaries as defined in Section 2 may be useful as a relative markers of the latitudinal location of the auroral zone "plasma sheet" plasma. They do not provide a definitive position of the polar cap boundary nor can they be used to infer the instantaneous width of the plasma sheet. However, in the absence of a clear identification of plasma sheet "edges", which is particularly difficult in the dawn local time sector, these boundaries provide useful flags for locating the position of UFI's and may prove equally useful in defining the relative locations of other auroral zone phenomena. The technique provided a successful ordering of UFI using relatively objective milestones which do not require an interpretation of the plasma features in terms of magnetospheric morphology. It is hoped that this method can be used equally well for comparing the relative positions of other auroral zone features.

We note several features about the UFI distributions. First, the observed occurrence distributions presented in Figures 5-7 must be regarded as lower limits to the frequency of auroral acceleration. The UFI technique and the selection criteria used here identify only those acceleration regions that generate UFI > 100 eV at altitudes below the spacecraft. Observations at higher altitudes (e.g. Collin et al., 1988) demonstrate that a significant amount of acceleration can occur above the Viking apogee.

One of the key results is that the "instantaneous" integrated width of UFI is typically 4 to 5 degrees in latitude (Figure 7). This is not surprising from examination of individual particle spectrograms that have been published over many years from various polar orbiting spacecraft. However the mapping of this extended acceleration region into the outer magnetosphere remains a challenge. In particular, models which assume that UFI are primarily generated within very narrow structures, such as are associated with discrete arcs, are difficult to reconcile with the data presented here.

A further result of interest in considering the magnetospheric context of the acceleration regions is the shape of the UFI latitudinal distribution with respect to the CIB (Figure 6). In particular, the distribution is quite symmetric about this boundary, as opposed, for instance, to rising to a cutoff at the boundary. This contrasts to the results of a similar study performed in the dusk local time sector using data from S3-3 (Ghielmetti et al., 1990). If one assumes that the CIB is, or is related to, a geophysically meaningful plasma boundary, then one might consider that the acceleration is related to processes occurring at or near to the boundary. It is hoped that future comparisons of these results with similar studies for other auroral zone phenomena will help to shed light on both the mapping into the outer magnetosphere and on the causality between the UFI regions and the plasma structures.

# REFERENCES

Cladis, J.B. and R.D. Sharp, Scale of electric field along magnetic field in an inverted V event, J. Geophys. Res., 84, 6564, 1979.

Collin, H.L., W.K. Peterson, J.F. Drake, and A.W. Yau, The helium components of energetic terrestrial ion upflows: their occurrence, morphology and intensity, J. Geophys. Res., 93, 7558, 1988.

Feldstein, Y.I., and Y.I. Galperin, The auroral luminosity structure in the high-latitude upper atmosphere: Its dynamics and relationship to the large-scale structure of the earth's magnetosphere, Rev Geophys., 23, 217, 1985.

Ghielmetti, A.G., R.G. Johnson, R.D. Sharp, and E.G.Shelley, The latitudinal, diurnal, and altitudinal distributions of upward flowing energetic ions of ionospheric origin, Geophys. Res. Lett., 5, 59, 1978.

Ghielmetti, A.G., J.M. Quinn, and R.N. Lundin, Extent and relative locations of auroral acceleration regions II: Pre-Midnight Sector, to be submitted to J. Geophys. Res., 1990.

Gorney, D.J., A. Clarke, D. Croley, J. Fennell, J. Luhmann, and P. Mizera, The distribution of ion beams and conics below 8000 km, J. Geophys. Res., 86, 83, 1981.

Heelis, R.A., J.D. Winningham, W.B. Hanson, and J.L. Burch, The relationship between high-latitude convection reversals and the energetic particle morphology observed by atmospheric explorer, J. Geophys Res., 85, 3315, 1980.

Mizera, P.F., J.F. Fennell, D.R. Croley Jr., A.L.Vampola, F.S. Mozer, R.B. Torbert, M. Temerin, R.L. Lysak, M.K. Hudson, C.A. Cattell, R.G. Johnson, R.D. Sharp, A.G. Ghielmetti, and P.M. Kintner ...... The aurora inferred f om S3-3 particles and fields, J. Geophys. Res., 86, 2329, 1981.

Sandahl, I., L. Eliasson, and R. Lundin, The hot plasma spectrometers on Viking, KGI Rep. 077, Kiruna Geophysical Institute, Feb. 1985.

Sharp, R.D., A.G. Ghielmetti, R.G. Johnson, and E.G.Shelley, Hot plasma composition results from the S3-3 spacecraft, in Energetic Ion Composition in the Earth's Magnetosphere, Ed. R.G. Johnson, Terra

Scientific Publishing Co., Tokyo, and D. Reidel, Dordrecht, Holland, 167, 1983.

Winningham, J.D., F. Yasuhara, S.-I. Akasofu, and W.J. Heikkila, The latitudinal morphology of 10 eV to 10 keV electron fluxes during magnetically quiet and disturbed times in the 2100-0300 MLT sector, J. Geophys. Res., 80, 3148, 1975.

Yau, A.W., B.A. Whalen, W.K. Peterson, and E.G. Shelley, Distribution of upflowing ionospheric ions in the high-altitude polar cap and auroral ionosphere, J. Geophys. Res., 89, 5507, 1984.

Yau, A.W., E.G. Shelley, W.K. Peterson, and L. Lenchyshyn, Energetic auroral and polar ion outflow at DE 1 altitudes: magnitude, composition, magnetic activity dependence, and long-term variations, J. Geophys. Res., 90, 8417, 1985.

# FIGURE CAPTIONS

FIGURE 1.   Invariant latitude and magnetic local time orbit tracks of Viking for the 89 auroral zone crossings analyzed in this study.

FIGURE 2.   Schematic spectrogram illustrating the energetic plasma boundary definitions used in this study. CEB and CIB are poleward boundaries of latitudinally contiguous fluxes at energies greater than 1 keV for electrons and ions respectively. PEB and PIB are poleward most limits of all fluxes with energies greater than 1 keV.

FIGURE 3.   Spectrogram of electron (top panel) and ion (bottom) panel fluxes during one of the orbits of the study period.

FIGURE 4.   Latitudinal locations of observed upflowing ions from each orbit are indicated by vertical bars. Many orbits contain multiple, distinct regions in which UFI were observed. The poleward boundary of contiguous isotropic energetic ions is indicated by the solid line. The poleward boundary of contiguous energetic electrons is denoted by shading below the boundary.

FIGURE 5.   Occurrence frequency of upflowing ions in 1 degree bins of invariant latitude. Background shading in 5 degree increments, is provided to guide the eye.

FIGURE 6   Occurrence frequency of upflowing ion in 1 degree bins relative to "instantaneous" position of poleward boundary of continuous energetic (1 keV) ions. The distribution with respect to this boundary is significantly more peaked than the raw distribution in invariant latitude (Figure 3).

FIGURE 7.   Occurrence frequency of the integrated latitudinal width of all regions of upflowing ions for each pass.

FIGURE 8.   Scatter plots with linear regression fits for the Continuous Ion Boundary vs the Continuous Electron Boundary (top panel); and for the Continuous Ion Boundary vs. the AE magnetic activity index (bottom panel).

FIGURE 9.   Scatter plot of integrated width of upflowing ion regions vs. magnetic activity index AE.
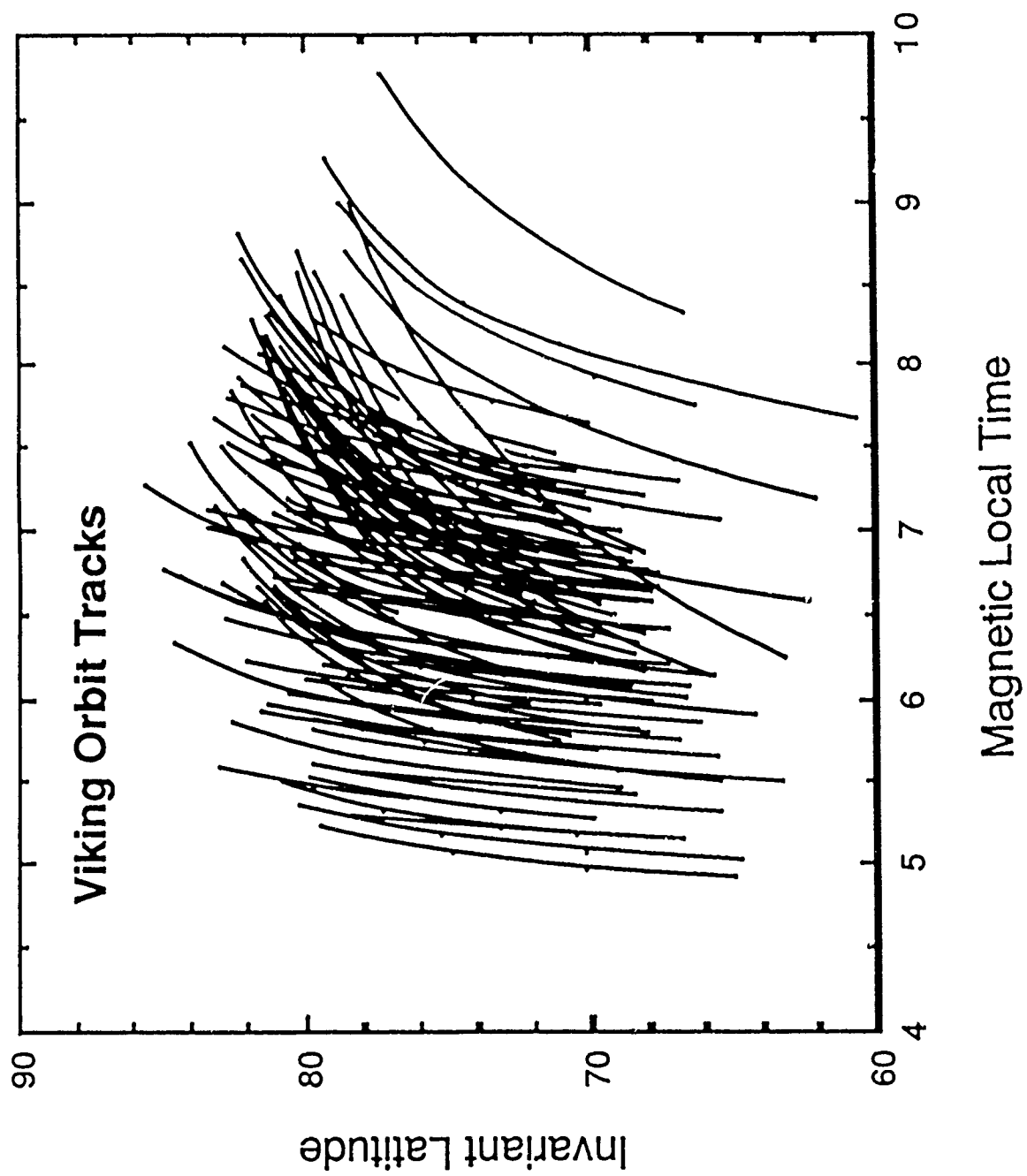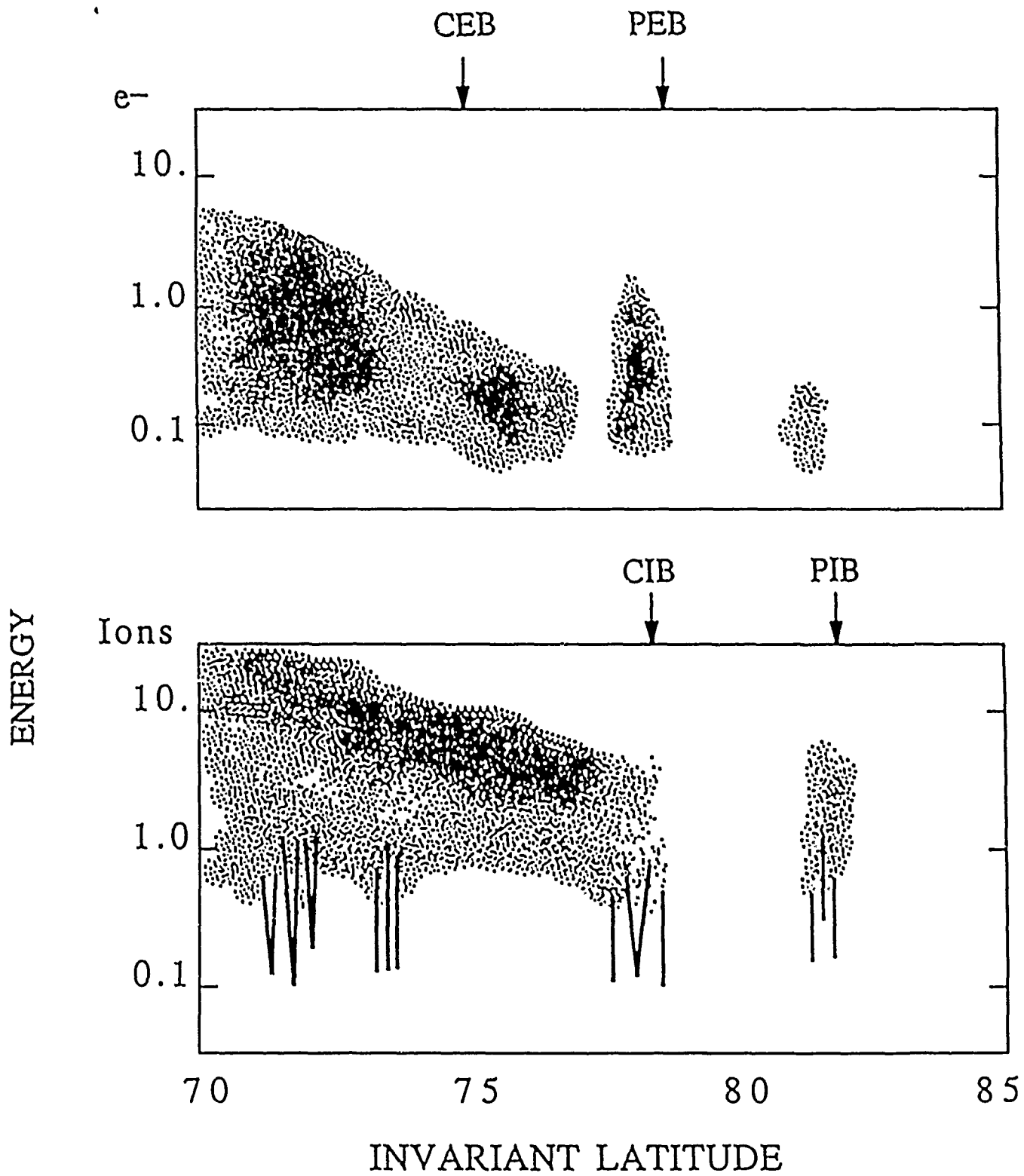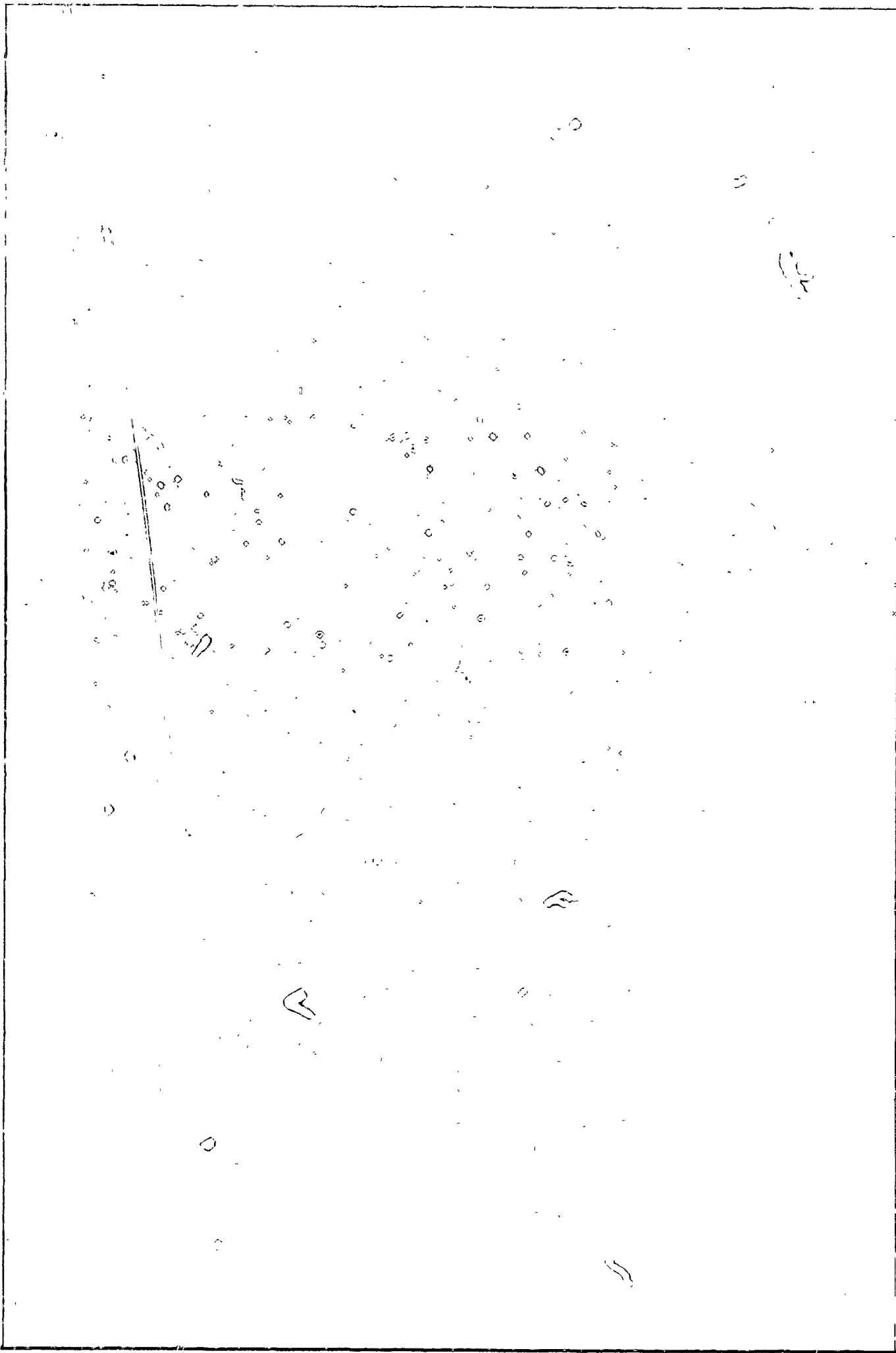
Viking Orbit Tracks

Invariant Latitude

Magnetic Local Time

Fig 1

Fig 2

Fig 4

A-15

Fig 5

Fig 6

A-17

Fig 7

Fig 8

A-19

Fig 9

A-20
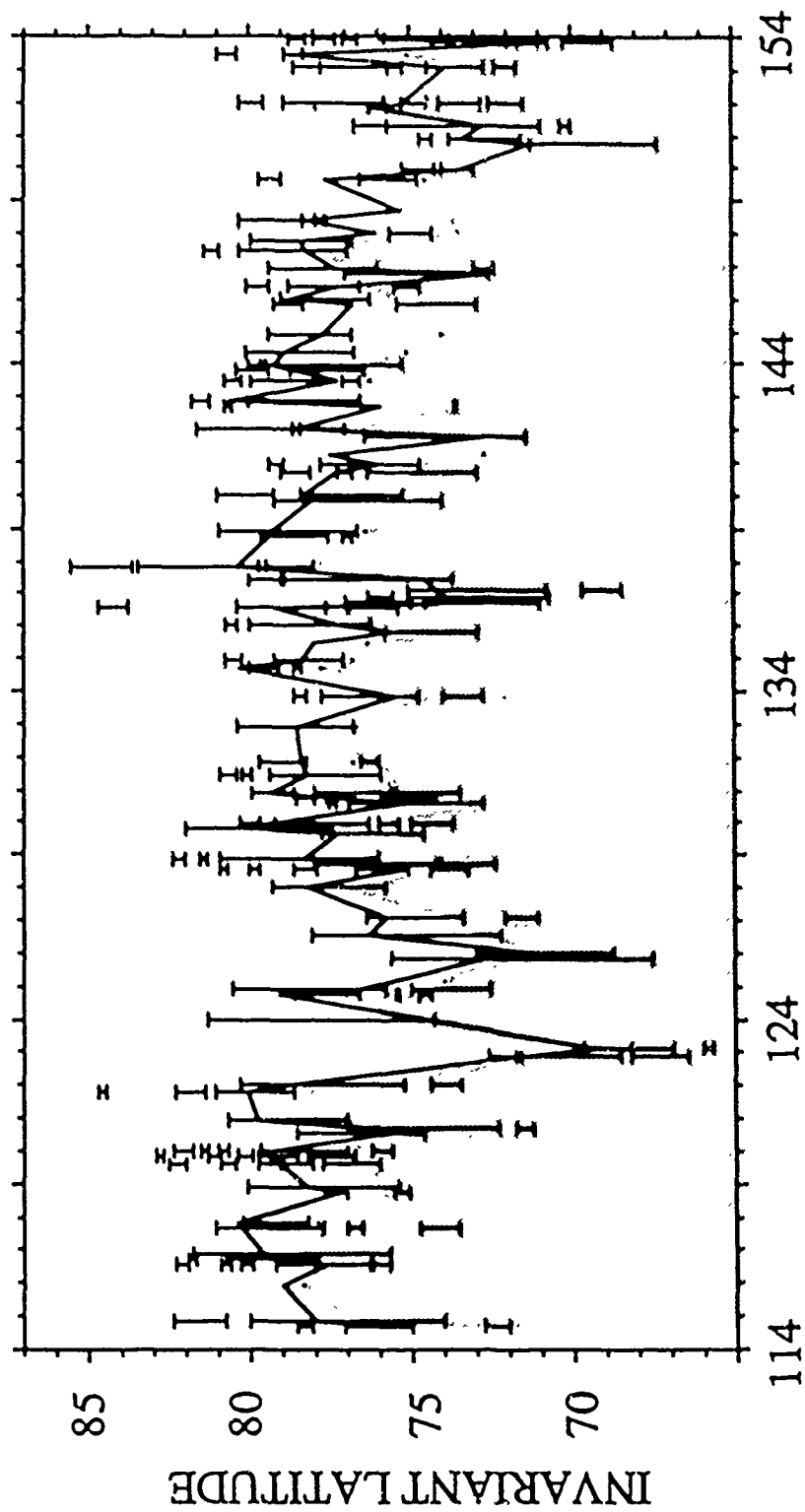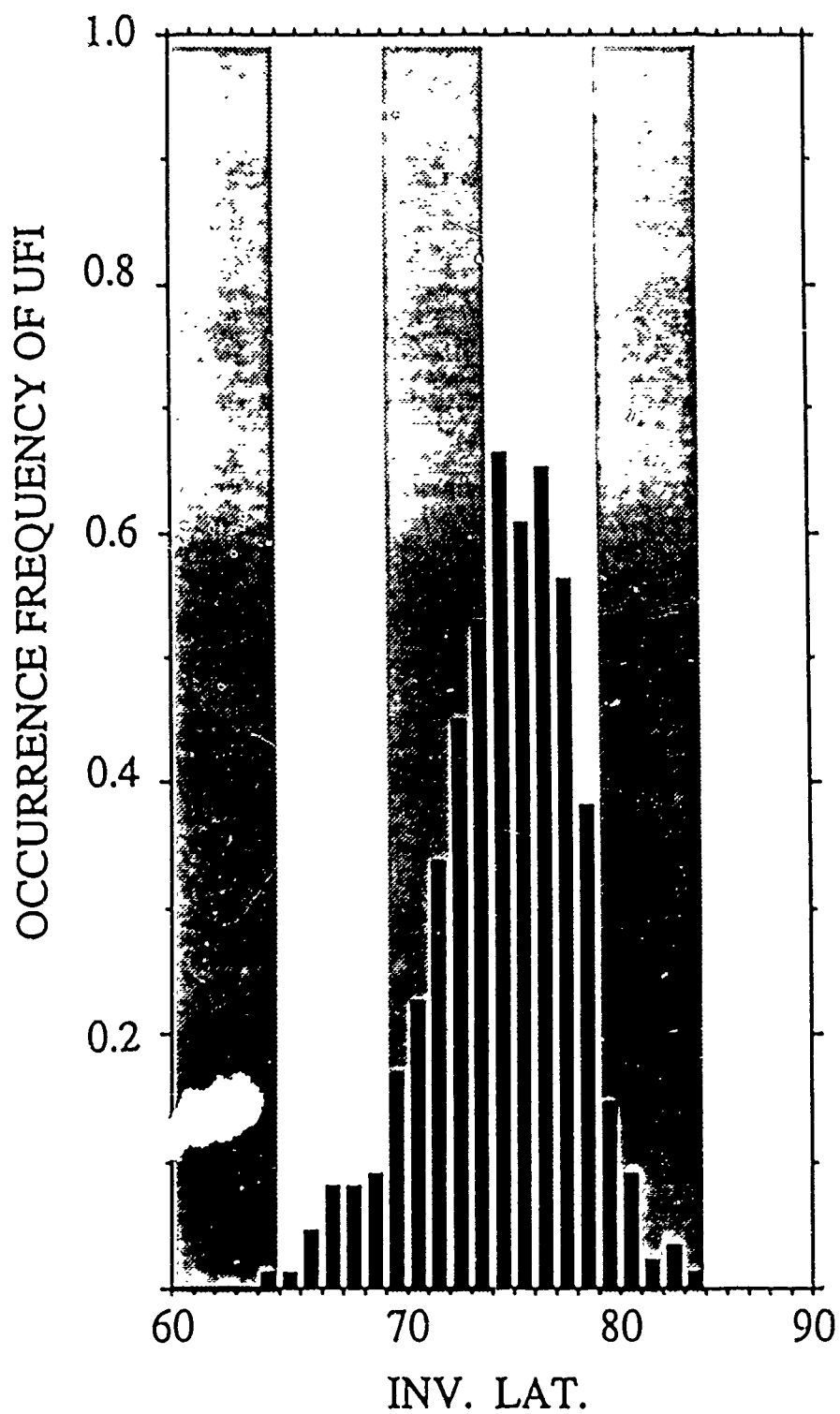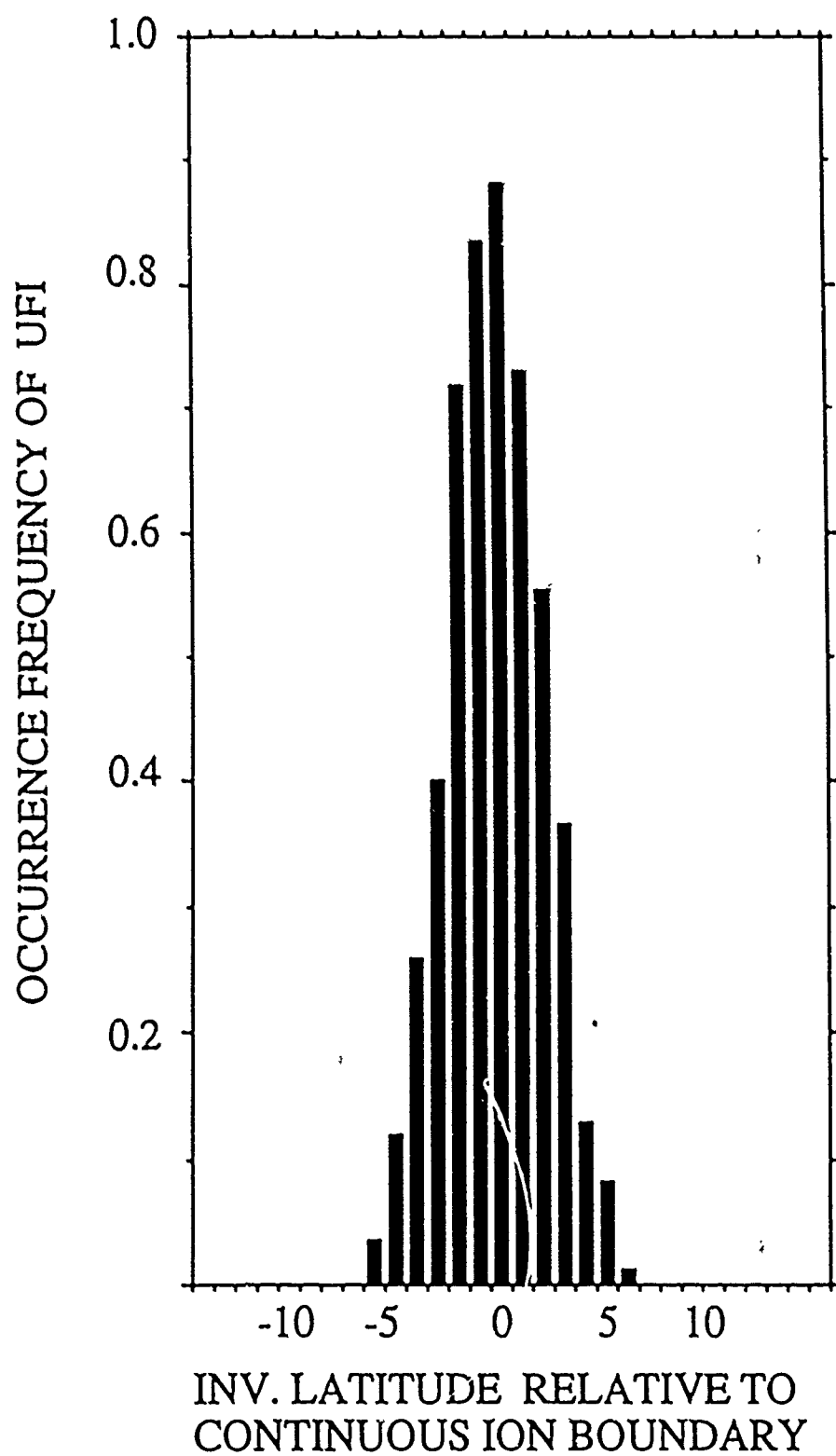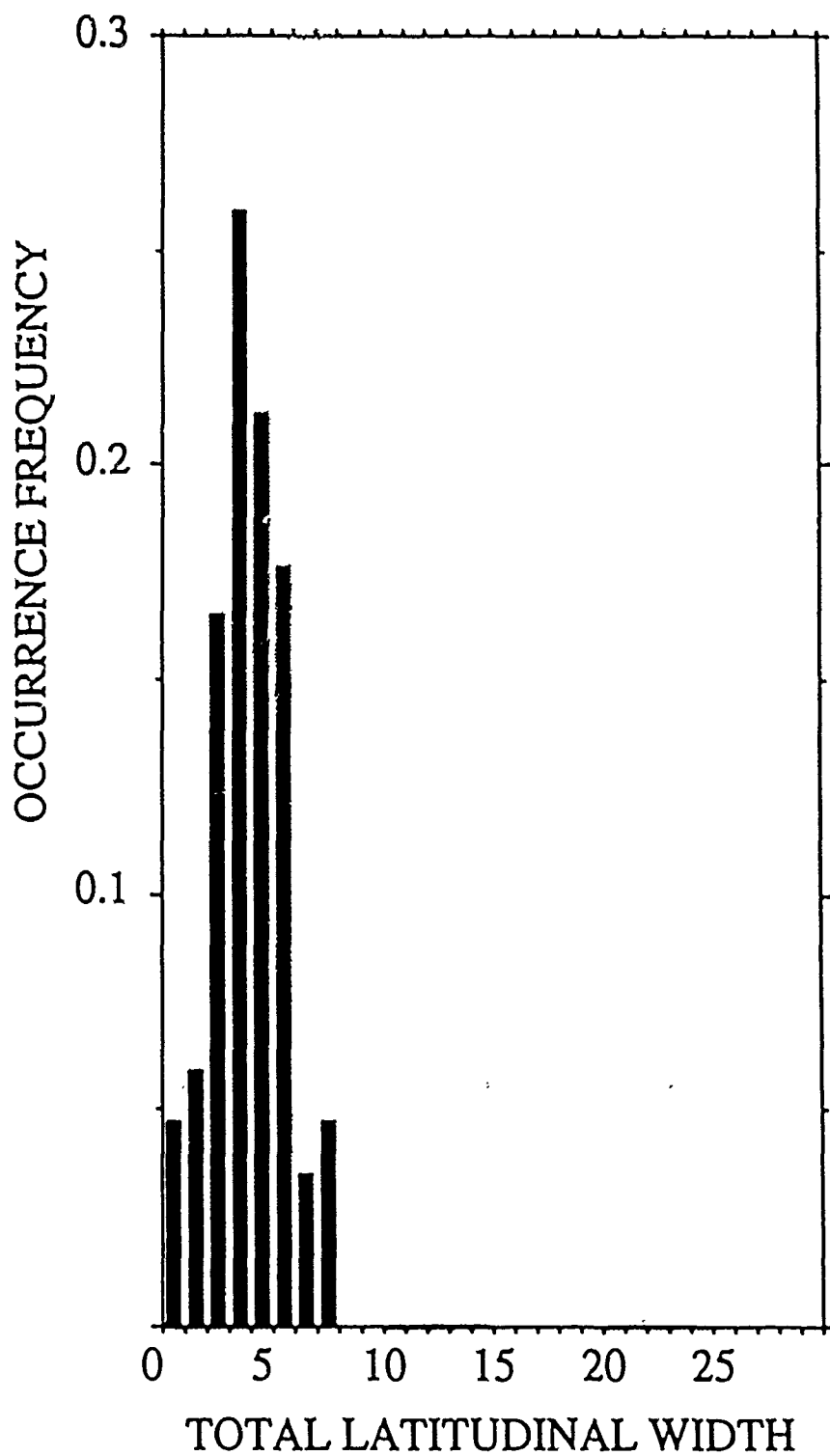
# APPENDIX  B


## ABSTRACTS
## OF
## PRESENTATIONS

# The Latitudinal Location and Extent of Ion Acceleration Regions in the Post-Midnight Sector.

J.M. Quinn, A. G. Ghielmetti (Lockheed Palo Alto Research Laboratory, 3251 Hanover St., Palo Alto, CA 94304)

R. N. Lundin, (Swedish Institute of Space Physics, Kiruna, Sweden)
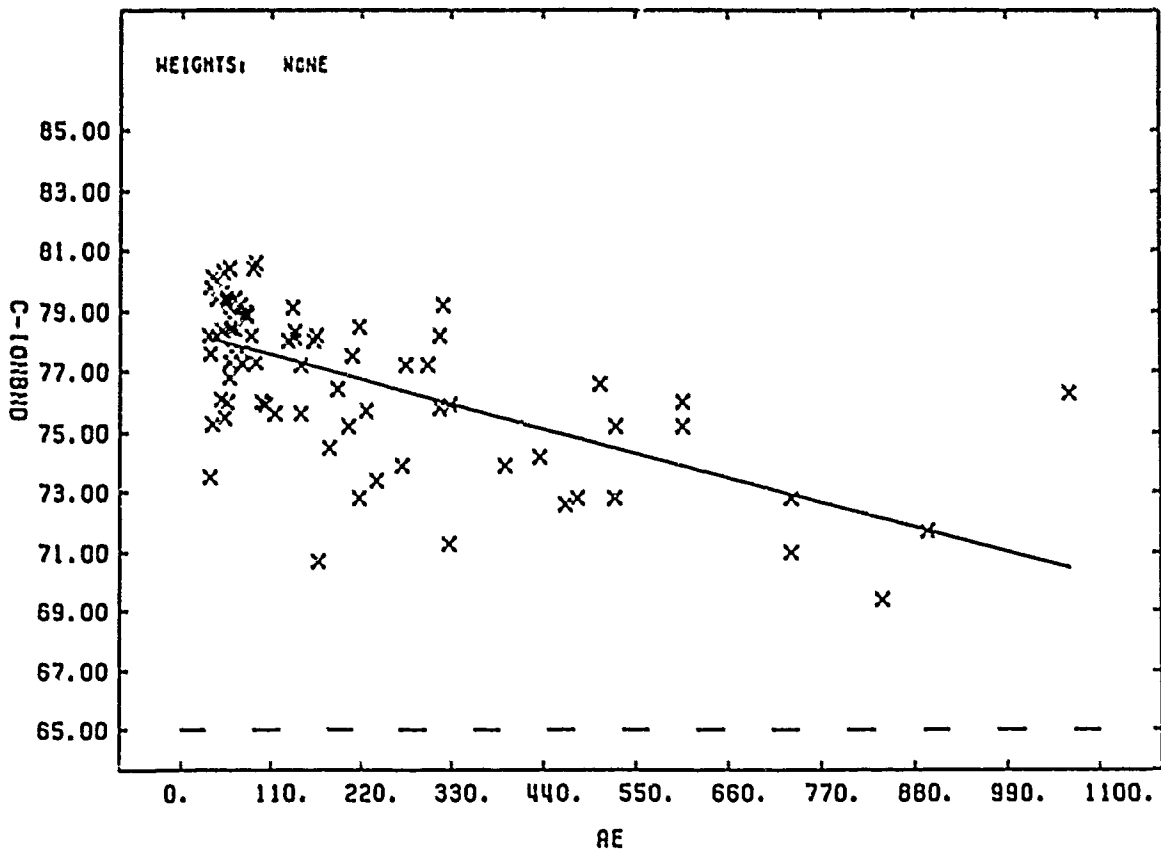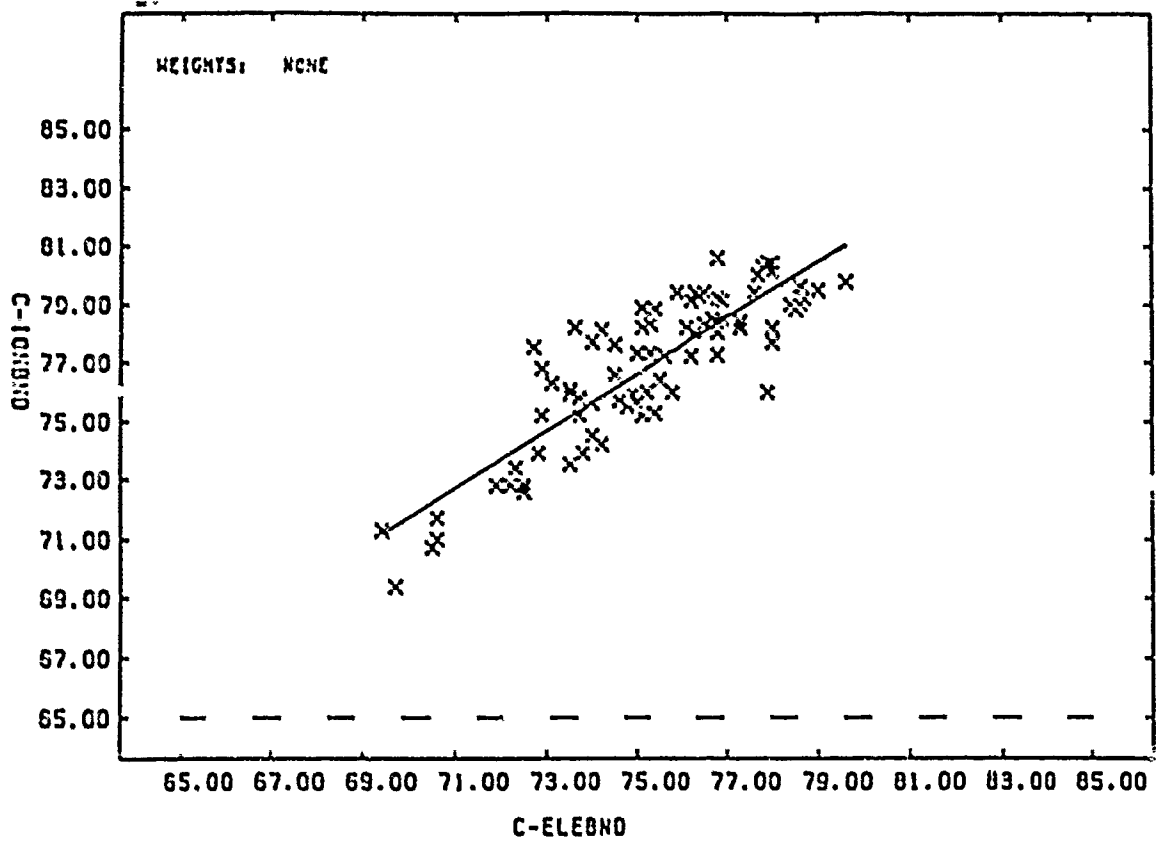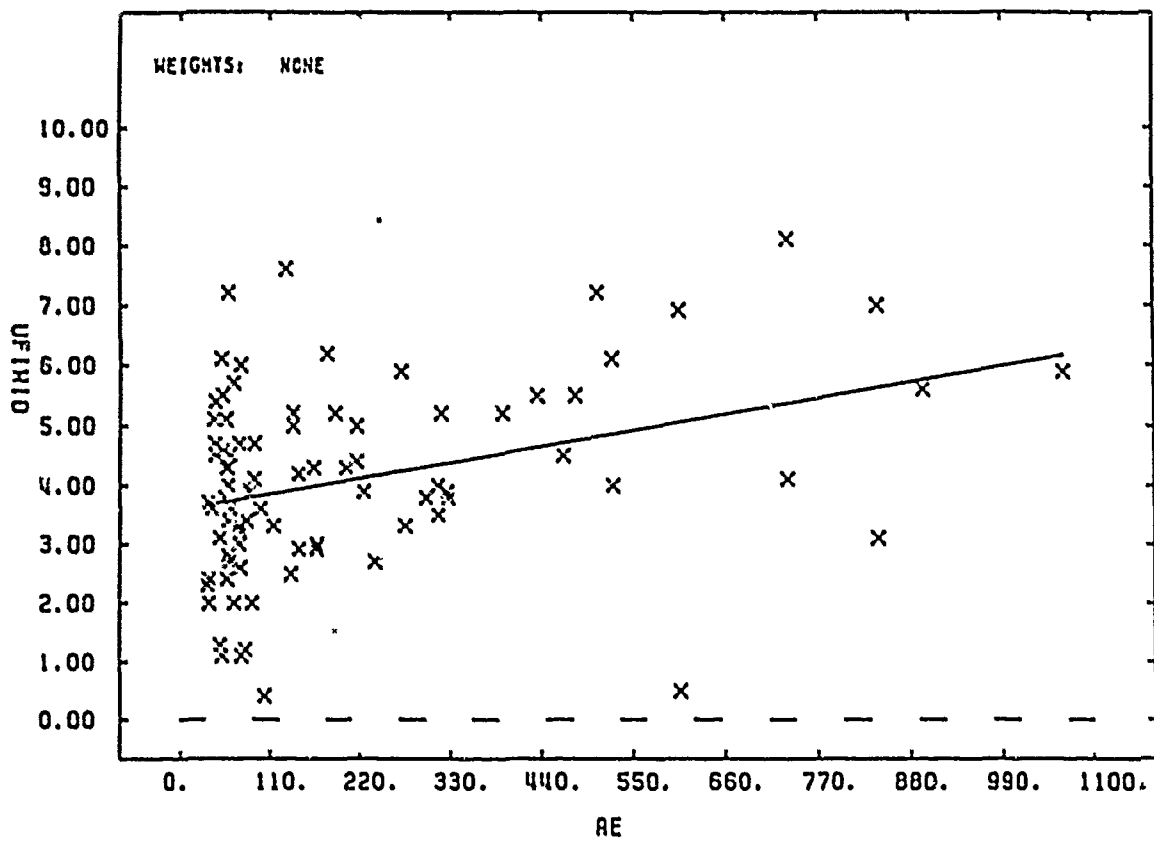
We report on the latitudinal distribution of accelerated upflowing ions as observed in a series of passes of the Viking satellite in the midnight to dawn local time sector. The location of upflowing ions is compared to various particle boundaries inferred from electron and ion signatures. On an orbit by orbit basis, the ion acceleration is found frequently to extend over a broad latitudinal range (several degrees). Typical upflowing energies are observed to be less than or on the order of 1 keV. The Viking results are compared with similar observations made from S3-3 in the dusk local time region which show ion acceleration regions occupying 50% or more of the latitudinal width of the plasma sheet approximately 1/3 of the time.

# Ion Heating by Broadband Low-Frequency Waves In The Cusp/Cleft

M. André (Swedish Institute of Space Physics, University of Umea, S-901 87 Umea, Sweden)
G. B. Crew (MIT Center for Space Research)
W. K. Peterson (Lockheed Palo Alto Research Laboratory)
A. M. Persoon (Department of Physics of Physics and Astronomy, University of Iowa)
C. J. Pollock (Space Sciences Laboratory, Marshall Space Flight Center)
M. J. Engebretson (Augsburg College)

Ion conic distribution functions are often observed in the cusp/cleft region of the dayside magnetosphere by the polar orbiting DE-1 and Viking satellites. We show that these ions can be heated by resonant interaction with broadband low-frequency (near the ion gyrofrequency) waves. Data from one crossing of the cusp/cleft by DE-1 is studied in detail. There is very good agreement between the onset of low-frequency waves and the onset of ion heating. Observed cool $O^+$ distributions and observed wave intensities are used as input to a Monte Carlo simulation. The theoretically obtained heated $O^+$ distributions are in good agreement with the corresponding observed distributions. The mean ion energies of about 200 eV obtained from the simulation agree well with several minutes of observations, corresponding to a distance of nearly 1000 kilometers along the satellite orbit. The $O^+$ distribution functions from both simulation and observations show that heating near the equatorward edge of the cusp/cleft region is rather local, while ions observed inside this region may be heated over altitudes of several thousand kilometers. This resonant heating by broadband low-frequency waves is important for the outflow of ionospheric ions into the magnetosphere.

# Coordinated Observations of Low Frequency Wave Turbulence and Ion Energization during a Magnetospheric Substorm

W. K. Peterson, H. L. Collin (Lockheed Palo Alto Research Laboratory, 3251 Hanover St., Palo Alto, CA 94304), G. B. Crew (Center for Space Research MIT), M. André (IRF, Umea, Sweden), J. Woch (IRF, Kiruna, Sweden), P.A. Lindqvist (Royal Institute, Stockholm Sweden), M. J. Engebretson (Augsburg College), A. M. Persoon (University of Iowa), and R. E. Erlandson (APL)

On May 4, 1986 near 1200 UT the Dynamics Explorer -1 Satellite crossed the mid-altitude ($r/Re \sim 4.6$) morning side auroral zone at 1700 magnetic local time. The onset of a magnetospheric substorm has been identified in the Viking images at 1153 UT. About 5 minutes later an intensification of low frequency (less than 2 Hz), magnetic and electric field turbulence was observed on both satellites. Perpendicularly energized, upflowing ion distributions were observed during the interval of intense wave turbulence on both satellites. The mass spectrometer on DE-1 showed that the heated ions on the morning side were primarily oxygen. No mass spectrometer information is available from Viking for this interval.

These observations suggest that the low frequency wave turbulence observed between $\sim$ 1156 and 1158 on both satellites energized upflowing oxygen ions by the ion cyclotron resonance mechanism and that the intensification of the turbulence at this time is a global feature related to the geomagnetic substorm.

# APPENDIX C

User's Guide to V3 Data Summary File Contribution

Rickard Lundin

Kiruna Geophysical Institute

## 1. Introduction.

The V3-DSF contains a summary of the ion and electron data from the Viking spacecraft. The data will be stored on the DSF-tape in such a form that a detailed analysis with physical parameters requires updated calibration factors and some simple computations described in Appendix 3. The idea of introducing separate computations for the moments of the distribution functions was to allow for a more flexible use of the V3-DSF data, as well as to facilitate the identification of erroneous data.

Since the particle data requires the magnetic field as a reference parameter, the V3-DSF also contains magnetometer data (the Bx,By and Bz components in the satellite frame of reference ) sampled every ≈ 1.2 s. The pitch angle of the particle fluxes can then be easily calculated from the scalar product formula given in Appendix 5.

## V-3 DSF Data Block.

A schematic of the V3-DSF data block structure is given in Appendix 1 and a more detailed description of the content is given in Appendix 2.

Each data block contains data sampled during ≈ 2.4 s for electrons (ESP 1, see eg the Viking blue book), positive ions (PISP1/2) and low energy $H^+$,$He^+$ and $O^+$ (from ICS1/2). The data block also contains some ion fluxes of selected masses from the time of flight mass spectrometer.

The ESP1 data section (word 10 to 17) consists of accumulated counts sampled in 16 energy levels within the energy range ≈ 0.01 to 40 keV. The accumulated counts are compressed in 8 bit words, the true total number of counts given by the formula in Appendix 2. The ESP1 spectral information is repeated twice in each data block. Thus electron spectral information will be given with a time resolution of ≈ 1.2 s , corresponding to a pitch angle interval of about 21°.

The PISP1/2 data section (word 18 to 25) has a data structure that is similar to the ESP1 section. Notice, however, that this data comes from two separate ion spectrometers with a great difference in conversion factor (see Appendix 3).

For both ESP1 and PISP1/2 data it is necessary to use separate energy tables depending on which working mode the instrument was in. The energy tables are tabulated in Appendix 4. Notice that the modes of operation can be determined by word 4 in the DSF data block. Particle fluxes can be deduced by the simple formula in Appendix 3.

Words 26 to 29 and 58 to 61 in the DSF data block gives some partial   .

moments of the electron distribution function (number flux and energy flux per unit solid angle within the energy range ≈ 0.01 – 40 keV) deduced every ≈ 0.6 s (consecutive readouts denoted "1" and "2" in Appendix 1).

Examples of how net currents, energy fluxes, mean energies, and number densities can be deduced from these partial integral quantities are given in Appendix 3.

In a similar way words 30 to 35 and 62 to 67 gives the partial integral quantities for ions of some selected masses integrated over the energy range ≈ 0.05 – 20 keV/e. The integration time is here ≈ 1.2 s. Notice that the partial integral quantities are written as 16 bit words using the special floating point algorithm in Appendix 2.

Words 36 to 41 and 68 to 73 in the DSF data block finally gives the time of flight data for some selected ions at energies > 30 keV. The energy level for each sample is represented by the E/q step word. Again notice that accumulated counts are obtained from the algorithm in Appendix 2 for 8 bits data.

## APPENDIX 1.
### V3 data summary file block (146 bytes/block)

word <----------- 16 bits --------------->

| # | | | |
|---|---|---|---|
| 1 | year | day | hour |
| 2 | min | | sec |
| 3 | msec | | |
| 4 | mode status | | |
| 5 | status error | | |
| 6 | mode change | | |
| 7 | magnetometer $B_x$ | | |
| 8 | magnetometer $B_y$ | | |
| 9 | magnetometer $B_z$ | | |

| # | left | right | |
|---|---|---|---|
| 10 | N = 1 | N = 2 | (42) |
| 11 | N = 3 | | (43) |
| 13 | | | |
| 14 | ESP 1 | ESP 1 | |
| 15 | data | data | |
| 16 | | | |
| 17 | N = 15 | N = 16 | |
| 18 | N = 1 | N = 2 | |
| | PISP 1 | PISP 1 | |
| | | N = 8 | |
| 22 | N = 1 | N = 2 | = 2.4 s |
| | PISP 2 | PISP 2 | |
| | | N = 8 | |

| # | | |
|---|---|---|
| 26 | Electron number flux 1 | |
| | Electron number flux 2 | |
| 28 | Electron energy flux 1 | |
| | Electron energy flux 2 | |
| 30 | $H^+$ number flux | |
| 31 | $He^+$ number flux | |
| 32 | $O^+$ number flux | |
| 33 | $H^+$ energy flux | |
| 34 | $He^+$ energy flux | |
| 35 | $O^+$ energy flux | |

| # | left | right |
|---|---|---|
| 36 | TOF $H^+$ (cts) | TOF Z > 1 |
| | TOF $O^+$ | TOF $He^+$ |
| | E/q step | HIT(M1+M2+A5) |
| | TOF $H^+$ (cts) | TOF Z > 1 |
| | TOF $O^+$ | TOF $He^+$ |
| 41 | E/q step | HIT(M1+M2+A5) |
| 42 | As above for frame 10 − 41 | |
| 73 | | |

## APPENDIX 2.
## V3-Data summary file.

| word | content |
|------|---------|
| 1 | bits 14-15 : year |
| | bits 5-13 : daynumber |
| | bits 0- 4 : hour |
| 2 | bits 6-15 : minute |
| | bits 0- 5 : second |
| 3 | milliseconds |

4
| bit 11 | : in flight calibration | (1 = on) |
|--------|--------------------------|----------|
| bit 10 | : preacceleration | (1 = on) |
| bit 8 - 9 | : mode status ESP | (0 - 2) |
| bit 6 - 7 | : mode status ICS1/2 | (0 - 3) |
| bit 4 - 5 | : mode status SECPISP | (0 - 3) |
| bit 2 - 3 | : mode status PISP | (0 - 2) |
| bit 0 - 1 | : mode status ICS3 | (0 - 3) |

5 status error ( =0 <=> no error)

bit 0 = 1 => ESP   bit 1 = 1 => PISP
bit 2 = 1 => ICS1/2   bit 3 = 1 => ICS3
bit 4 = 1 => SECPISP

6 mode change ( =0 <=> no change)

bit 0 = 1 => ESP mode changed   bit 1 = 1 => PISP mode ch.
bit 2 = 1 => ICS1/2 mode ch.   bit 3 = 1 => ICS3 mode ch.
bit 4 = 1 => SECPISP mode ch.

| word | content |
|------|---------|
| 7 | $B_x$ magnetometer |
| 8 | $B_y$ magnetometer |
| 9 | $B_z$ magnetometer |
| 10 - 17 | : ESP1 data (8 bits data) |
| 18 - 21 | : PISP1 data (8 bits data) |
| 22 - 25 | : PISP2 data (8 bits data) |
| 26 | Electron number flux ( at time = $t_0$ , 16 bits data) |
| 27 | Electron number flux ( at time = $t_0$+0.59 s , 16 bits data) |
| 28 | Electron energy flux ( at time = $t_0$ , 16 bits data) |
| 29 | Electron energy flux ( at time = $t_0$+ 0.59 s , 16 bits data) |
| 30 | $H^+$ number flux (16 bits data) |
| 31 | $He^+$ number flux (16 bits data) |
| 32 | $O^+$ number flux (16 bits data) |
| 33 | $H^+$ energy flux (16 bits data) |
| 34 | $He^+$ energy flux (16 bits data) |
| 35 | $O^+$ energy flux (16 bits data) |
| 36 - 41 | MICS/Y data (8 bits data) |
| 42 - 73 | As above for word 10 - 41, starting time($t_0$) =1.185 s after time defined in word 1 - 3 |

Word 1 - 73 is repeated 56 times per record

8 bits data: value = (IAND(IV,15)+16.)*2**IAND(ISHFT(IV,-4),15)-16.

16 bits : value = (IAND(IV,1023)+1024.)*2**IAND(ISHFT(IV,-10),63)-1024.

## APPENDIX 3

### Energy levels for ESP1 and PISP1/2:

| | ESP1 (keV) | | | PISP1 | PISP2 |
|---|---|---|---|---|---|
| N | Mode 0 | Mode 1 | Mode 2 | (keV) | (keV) |
| 1 | 0 | 0.09 | 0.25 | 0.057 | 1.84 |
| 2 | 0 | 0.16 | 0.33 | 0.090 | 2.89 |
| 3 | 0.015 | 0.24 | 0.42 | 0.139 | 4.46 |
| 4 | 0.14 | 0.37 | 0.57 | 0.216 | 6.92 |
| 5 | 0.32 | 0.55 | 0.79 | 0.334 | 10.7 |
| 6 | 0.60 | 0.78 | 1.05 | 0.520 | 16.7 |
| 7 | 1.03 | 1.20 | 1.30 | 0.806 | 28.8 |
| 8 | 1.65 | 1.75 | 1.85 | 1.25 | 40.0 |
| 9 | 2.60 | 2.50 | 2.65 | | |
| 10 | 3.90 | 3.90 | 3.90 | | |
| 11 | 5.60 | 5.60 | 5.60 | | |
| 12 | 8.20 | 8.20 | 8.20 | | |
| 13 | 11.9 | 11.9 | 11.9 | | |
| 14 | 18.2 | 18.2 | 18.2 | | |
| 15 | 25.2 | 25.2 | 25.2 | | |
| 16 | 36.5 | 36.5 | 36.5 | | |

### Conversion from counts to fluxes:

Flux $(cm^{-2} s^{-1} sr^{-1} keV^{-1})$:  $\quad J(E,\beta) = R(E,\beta) / \ldots / t_s$

Number Flux $(cm^{-2} s^{-1} sr^{-1})$:  $\quad \beta(\beta) = N_\beta(\beta) * K_1$

Energy Flux $(erg\ cm^{-2} s^{-1} sr^{-1})$:  $\quad F(\beta) = N_F(\beta) * K_2$

where:

$$N_\beta(\beta) = \int_{E1}^{E2} J(E,\beta)\ dE$$

$$N_F(\beta) = \int_{E1}^{E2} E * J(E,\beta)\ dE$$

ß is the pitch angle, E is the energy, $t_s$ is the accumulation time, R(E,ß) is accumulated counts in the energy channnel E and pitch angle ß, C(E) is the conversion factor, N(ß) is the number of counts integrated over the entire energy interval of the spectrometer, and $K_1$ and $K_2$ are constants.

### Preliminary Conversion factors, constants and viewing directions.

ESP1:  $C(E) = 5.7*10^{-5}*E$  $(cm^2\ sr\ keV/cts)$ ; E in keV
$K_1 = 1.$
$K_2 = 1.602*10^{-12}$
$t_s = 0.074\ s$
$\underline{s} = (0.866,-0.500,0)$

PISP1:  $C(E) = 1.8*10^{-3}*E$  $(cm^2\ sr\ keV/cts)$ ; E in keV
$t_s = 0.149\ s$
$\underline{s} = (0.866,-0.500,0)$

PISP2:  $C(E) = 1.4*10^{-4}*E$  $(cm^2\ sr\ keV/cts)$ ; E in keV
$t_s = 0.149\ s$
$\underline{s} = (0.866,-0.500,0)$

ICS1/2:  $K_1 = 1.$
$K_2 = 1.602*10^{-12}$
$\underline{s} = (0,1.,0)$

### Pitch angle calculation.
The pitch angle is obtained by simply taking the dot product of the instrument viewing direction $\underline{s}$ and the magnetic field vector $\underline{B}$ in the magnetometer frame of reference:

$$ß = \cos^{-1}(\underline{s} \cdot \underline{B}/B\cdot)$$

where    $B\cdot = (B_x^2 + B_y^2 + B_z^2)^{1/2}$

and    $\underline{B} = (B_x, B_y, B_z)$

### Moment Calculations.
Preliminary values of some hot plasma moments and other related plasma quantites can be obtained from the V3-DSF using the following formulas:

Number density (N) is obtained from:

$$N = C_1 \int_0^- \int_0^\pi J(E,\beta) \, E^{-1/2} \, \sin\beta \, d\beta \, dE \qquad (cm^{-3})$$

where $C_1 = 1.06 \times 10^{-12}$, E is in eV, $\beta$ is the pitch angle and the integrations are performed by summing over the 16 energy intervals and 8 to 9 pitch angle intervals.

$$\left( eg \quad N = C_1 \sum_{i=1}^{16} \sum_{k=1}^{8} J(E_i,\beta_k) \, E_i^{-1/2} \, \sin\beta_k \, \Delta\beta_k \, \Delta E_i \quad \right)$$

Number flux ($\beta$) is obtained from:

$$\beta = \pi \int_0^\pi \beta(\beta) \, \sin2\beta \, d\beta \qquad (cm^{-2} \, s^{-1})$$

A nonzero value of $\beta$ means a net transport of particles ( within the energy range of the measured species) parallel or antiparallel to the magnetic field direction. Parallel currents can be deduced from the formula:

$$I_1 = 1.602 \times 10^{-19} \, ( \beta_p - \beta_e)$$

where the subscript "p" and "e" stands for positive ions and electrons respectively.

Energy flux ($\mathcal{E}$) is obtained from:

$$\mathcal{E} = \pi \int_0^\pi \mathcal{F}(\beta) \, \sin2\beta \, d\beta \qquad (erg \, cm^{-2} \, s^{-1})$$

As for the number flux, a nonzero value of the energy flux means a net transport (up or down) of energy flux.

Notice that a calculation of the particle deposition into the upper atmosphere requires knowledge of the loss cone half angle ($\beta_c$), as well as a detailed knowledge of eg acceleration processes between the satellite and the upper atmosphere.

Finally the mean energy of the particle flux can be obtained from:

$$\langle E \rangle = \mathcal{F}(\beta) / \beta(\beta) \times 6.24 \times 10^{11} \qquad (eV)$$

# APPENDIX  D


"The Viking Program"

# The Viking Program

## The Viking Science Team[1]

### Introduction

Sweden's first satellite, Viking, was successfully launched on February 22, 1986, at 01:44 UT. It was carried into orbit with the French remote sensing satellite SPOT by an Ariane 1 booster, launched from French Guiana. Viking's perigee boost motor placed this relatively small satellite (~520 kg) into a final 817 km × 13,527 km polar orbit, where it is conducting scientific observations of complex plasma processes in the magnetosphere and ionosphere of the earth. The satellite carries experiments to measure electric fields, magnetic fields, charged particles, waves, and auroral images. These experiments were sup-

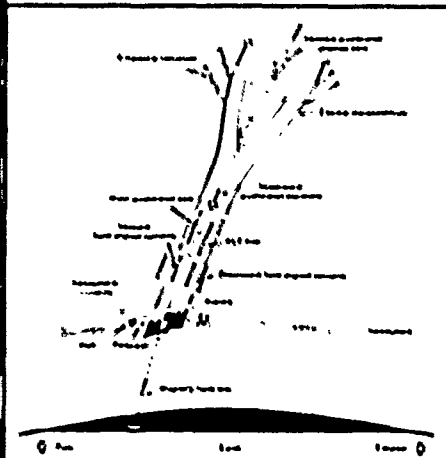[1]The members of the Viking Science Team are listed in Table 3.



Fig. 1. A schematic view of the complex plasma processes occurring on the geomagnetic lines that couple the magnetosphere and auroral ionosphere (adapted from Science Definition Working Group, 1979]. Viking appears to have passed over a similar region of upward flowing ions and wave activity during an orbit on March 25, 1986, at approximately 20:40 UT and at a 7000 km altitude. These data are discussed further in the article.

Cover. Artist's view of Sweden's first satellite, Viking, in polar orbit above the earth. Viking was launched into a 817-km × 13,527-km polar orbit on February 22, 1986, by an Ariane 1 booster and is presently conducting measurements of space plasma phenomena in the auroral and polar regions. The location of the Esrange ground station near Kiruna, Sweden, is indicated by the red dot. For more information on the Swedish spacecraft and its associated scientific experiments, see the article "The Viking Program" by the Viking Science Team, p. 793. Results from the Viking mission will also be presented at the AGU Fall Meeting/ASLO Winter Meeting on Monday, December 8, 1986. For details on scheduling, see the meeting summary chart on pages 799–802.

plied by scientific teams from Sweden, Canada, Denmark, France, Norway, the United States, and the Federal Republic of Germany. All booms have been deployed, all experiments have been activated and checked out, and they are now conducting measurements.

Telemetry data from Viking are received and processed on a real time basis at the Esrange tracking station located near Kiruna, Sweden, above the Arctic circle (the red circle on the cover illustration). These data are reduced and displayed by computer graphics techniques immediately after reception at the ground station. Scientists engage in collaborative analysis of the space plasma phenomena at nearly the instant they are observed. Special "campaigns" are conducted that focus on special scientific topics and coordinated observations are made with surface, balloon, rocket and other satellite programs. The Viking program is unique because experiment

#### TABLE 1. Viking Orbit Parameters

| Parameter | Value |
|---|---|
| Time of launch | 01:44:35 UT* |
| Apogee altitude, km | 13,527 km |
| Perigee altitude, km | 817 km |
| Period | 262 min (4.4 hrs) |
| Inclination | 98.8° |

Apogee over North Pole region in Summer 1986; over South Polar Region in Summer 1987.

*On February 22, 1986

modes can be changed on a nearly real-time basis in order to concentrate on special phenomena that may be occurring at the moment. Another unique feature of this program is the data distribution system to the international community of scientists. A series of quick look plots (QLP) is produced and distributed on a weekly basis to any scientist in the world for a small charge. These plots contain summaries of the information acquired by all Viking instruments. The goal is to inspire interest in the Viking data from the international scientific community.

### Scientific Objectives

Northern Scandinavia is among the most favorable places on earth to measure phenomena related to the coupling of energy between the sun and outer space with the lower atmosphere and ionosphere. This is because the auroral zones are the focal points for this energy deposition, which can reach $10^{11}$ watts. The most spectacular manifestation of this phenomena is the northern lights or aurora, which have been studied for centuries by Scandinavian scientists such as Anders Celsius, Kristian Birkeland, Christopher Hansteen, Anders J. Ångström, and Hannes Alfvén.

The auroral regions encompass a dynamic and complex system of plasmas that interact with magnetic fields and electric currents. Figure 1 is a schematic view of some of these complicated phenomena; Viking appears to have passed over this type of configuration. The Viking program is directed at understanding large-scale phenomena, such as plasma convection, global current systems, and auroral morphology, as well as small-scale and microphysical problems, including parti-
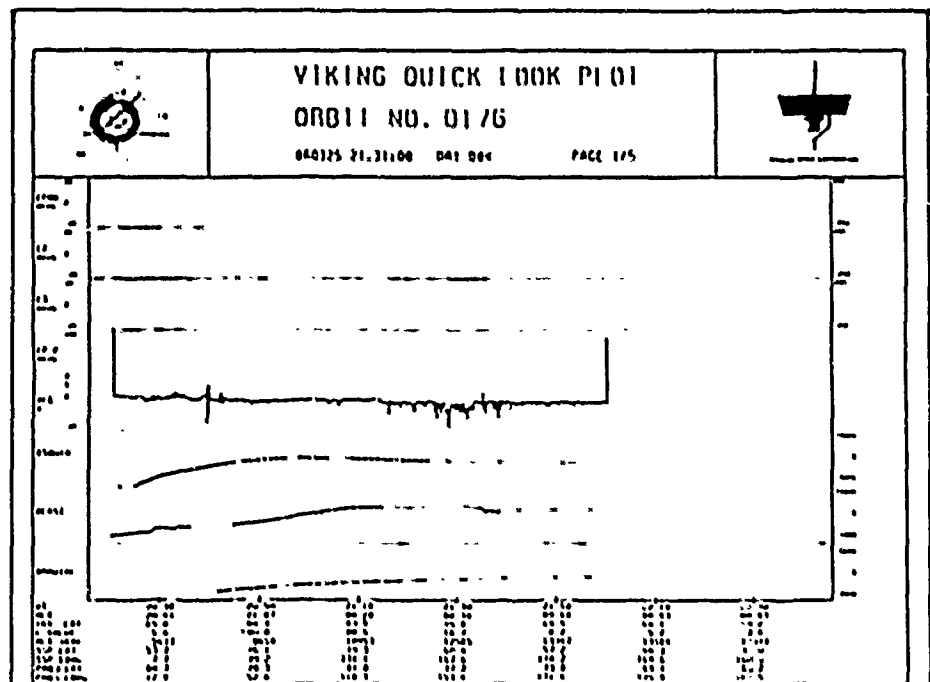


Fig. 2. An example of the first page of the five-page set of Viking QLPs for orbit 176 on March 25, 1986. These plots are produced within a few hours of the data acquisition at the Esrange ground station. This is the preliminary form of the Viking data that is being distributed to the international scientific community. See the text for details of these data.
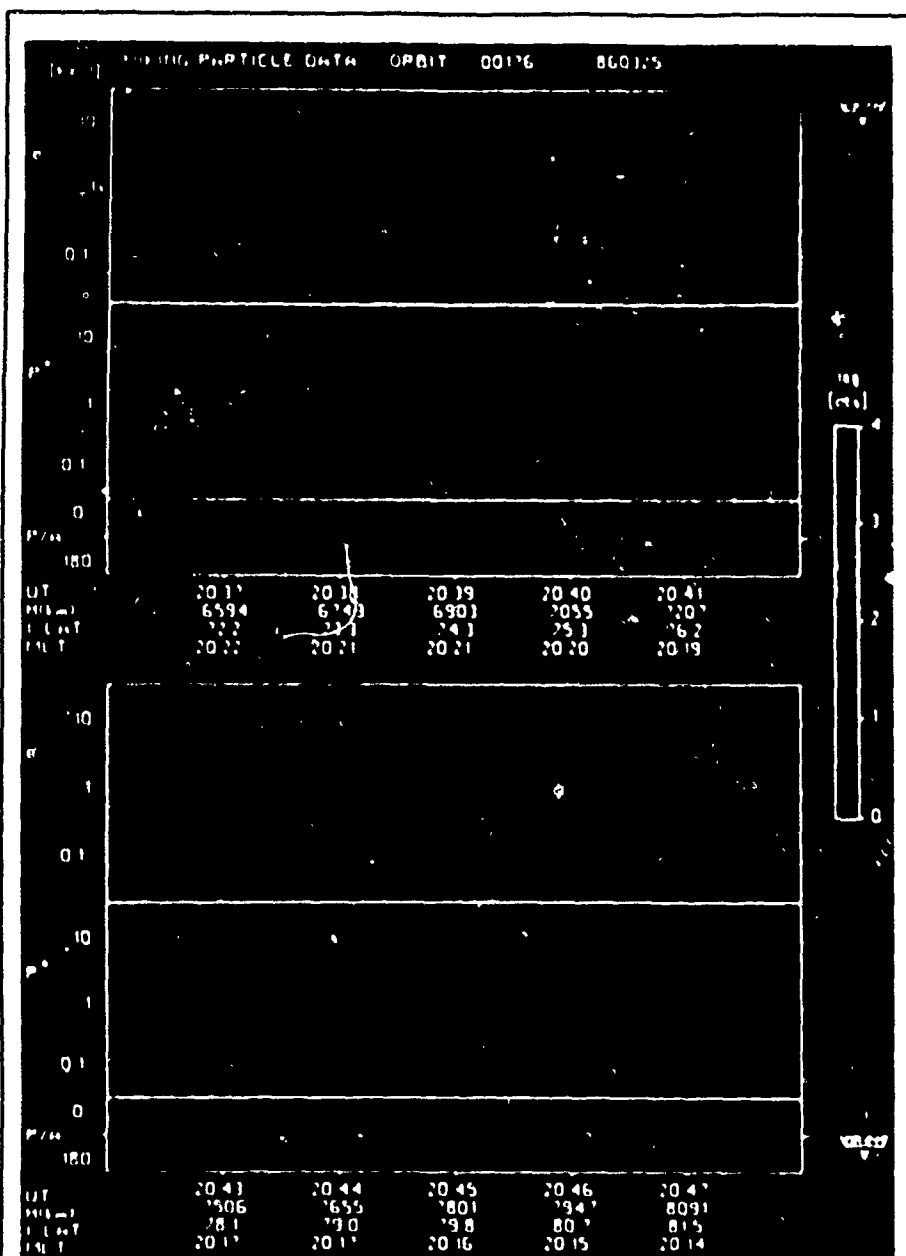
*Fig 3.* Energy-time spectrogram of data from the particle experiment (V3) during the Viking crossing of the evening auroral zone on March 25, 1986, as shown in Figure 2.

Power is supplied by eight body-fixed solar arrays, with a battery providing backup power during eclipses. Telemetry is provided by an S band link at a 55-kbit/s data rate. Data are received on a real-time basis at the Esrange ground station. A spin rate of 3 rpm is maintained by magnetic coil torquers commanded from the ground. Some orbit characteristics for Viking are listed in Table 1.

## The Viking Scientific Instruments

### V1: Electric Field Experiment

The dc electric field is measured by three orthogonal pairs of spherical probes. The probes are mounted in the tips of four 40-m wire booms in the spin plane of the satellite and at the tips of two rigid 4-m axial booms along the spin axis. This allows the possibility of measuring the instantaneous three-dimensional electric field vector. One pair of probes in the spin plane is also used, on a time-sharing basis with the Low-Frequency Wave Experiment (V4L), to measure plasma density fluctuations. The sampling rate of the V1 experiment is either 53 or 106 samples per second.

### V2: Magnetic Field Experiment

The Viking Magnetic Field Experiment includes a fluxgate magnetometer system with the sensors mounted on a 2-m radial boom to reduce spacecraft related measurement errors. The experiment has four automatically switchable ranges, from $\pm 1024$ nT to $\pm 65,536$ nT (full scale) and resolutions commensurate with a 13-bit analog to digital (A/D) converter in each range ($\pm 0.25$ nT to $\pm 8$ nT). Approximately 53 vector samples are acquired per second. This experiment is similar to the AMPTE/CCE (Active Magnetospheric Particle Tracer Explorer/Charged Composition Explorer) magnetic field experiment, except that the latter instrument has three additional ranges, extending to $\pm 16$ nT [*Potemra et al.*, 1985]. The Viking Magnetic and Electric Field Experiments (V1 and V2) can be sampled at the same rate (53 samples per second) to determine whether the variations are due to fine-scale currents or waves.

### V3: Hot Plasma Experiment

The particle experiment consists of a large number of instruments that allow measurements of

- electrons with spectral resolution $\Delta E/E \sim 0.05$, from 10 eV to 40 keV;
- electrons with angular resolution $\Delta \alpha \leq 2°$ from 0.1 keV to 300 keV;
- energy and pitch angle distributions of ions $\Delta E/E \sim 0.08$, $\Delta \alpha \leq 6$ from 40 eV to 40 keV;
- three-dimensional distribution functions of ions from the satellite potential to 10 keV; and
- composition, energy, and pitch angle distribution of ions up to 10 MeV/nucleon.

All these measurements can be made simultaneously.

### V4L: Low-Frequency Wave Experiment

The wave experiment is divided into two parts, depending upon the frequency. The Low-Frequency Experiment (V4L) measures
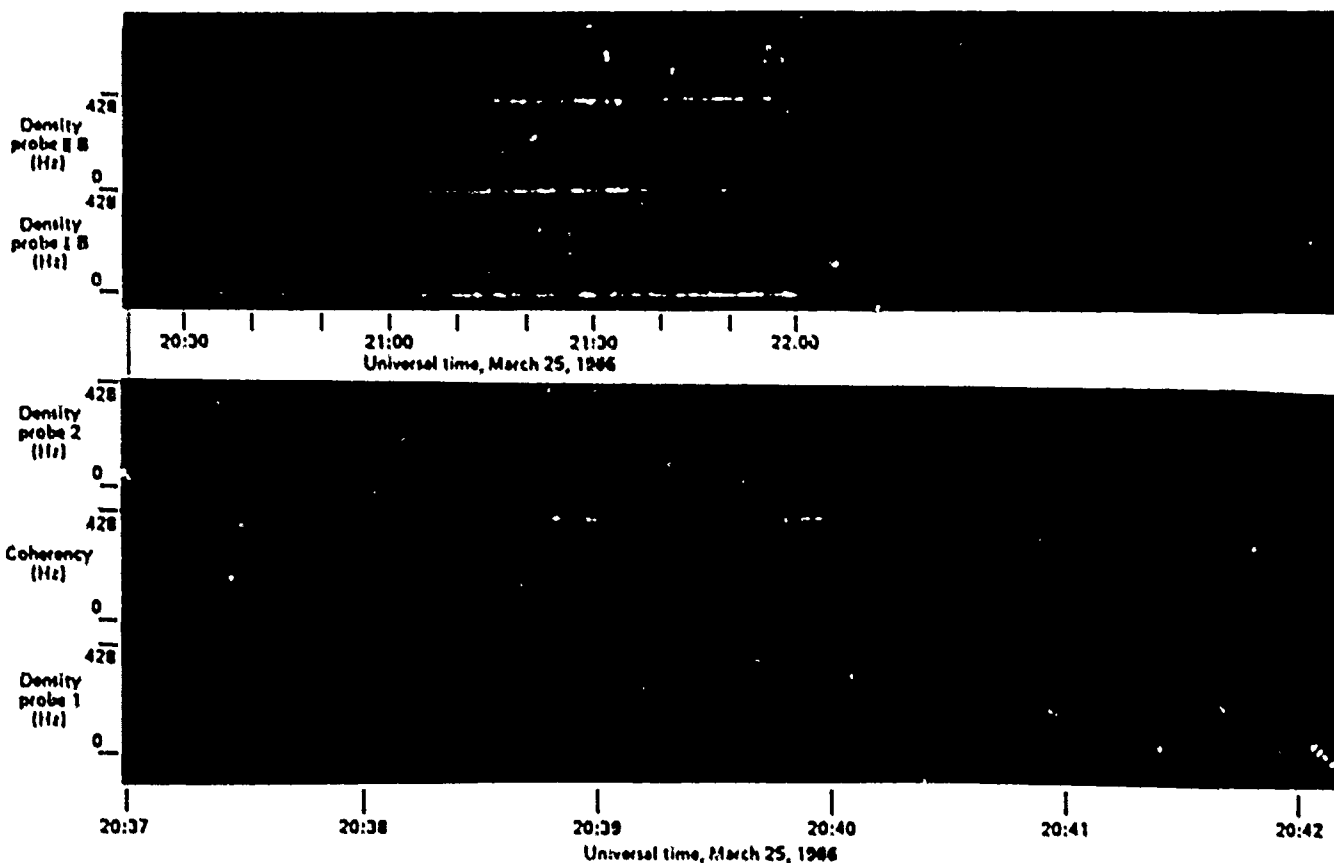
cle acceleration processes, wave-particle interactions, shock structure, fine-structured currents, and auroral kilometric radiation (AKR). Viking was specifically designed to perform high-resolution measurements of electric fields, magnetic fields, energetic particles, plasma waves, and ultraviolet emissions. The orbit was chosen to sample the auroral plasmas at intermediate altitudes (1–2 $R_t$) that are not usually explored by satellites and where a wealth of interesting processes is predicted to occur, including the key mechanisms responsible for the acceleration of auroral particles. The Viking spacecraft and its complement of instruments are described and some examples of the recently acquired data are presented in this article.

## The Viking Spacecraft

The Viking spacecraft in its deployed configuration is illustrated on the cover. This drawing shows the two 2-m-long radial booms used for the magnetic field and plasma wave experiments. Also shown are the four 40-m-long wire booms and two 4-m-long axial booms used for the electric field experiment. The fluxgate magnetic field sensor is located at the end of the thick boom pointing up, and the search coil magnetometer sensor is located at the end of the thick boom pointing down. The "whisk-shaped" plasma wave antennas are located near the end of each rigid boom. The satellite's spin axis is perpendicular to the two rigid booms and is approximately horizontal in the cover drawing. The particle detectors and UV imager cameras are located with the solar panels along the many-sided outside edge of the satellite, and their fields of view are directed radially away. In its stowed launch configuration, Viking was about 0.5 m high and 2 m in diameter; it weighed 520 kg, including 263 kg for the perigee boost motor.

*Fig. 4.* Spectrogram of data from the Low-Frequency Wave Experiment (V4L) during Viking orbit 176 on March 25, 1986. The top two panels show spectra for the entire 100-minute pass, and the bottom three panels show spectra and coherency for a 5-minute segment.

waves up to about 10 kHz. V4L can process simultaneously two wave signals that may come from any of the electric field antennas, from a magnetic loop antenna measuring fluctuations in the direction of the spin axis, or from the V1 experiment. One of the two signals can be processed by an onboard DFT (digital Fourier transform) analyzer and a filter bank comprising three filters. The wave form of both of the signals can be sampled with the Nyquist frequency of 214 Hz or 428 Hz. V4L also measures the plasma density by sweeping one of the density probes.

### V4H: High-Frequency Wave Experiment

The High-Frequency Wave Experiment (V4H) has two sets of eight filters each, with center frequencies from 4 kHz to 512 kHz, and a pair of stepped frequency analyzers from 10 kHz to 500 kHz. Analog signals are provided by one of the electric field antennas or from the magnetic loop antenna. There are also mutual impedance and resonance sounder experiments for measurements of the plasma density. The high-frequency signal can be fed through the DFT-analyzer of V4L. This increases the frequency resolution from 1 kHz to 100 Hz for studies of the fine structure of AKR.

### V5: Ultraviolet Auroral Imager

An important link between the ground-based and satellite-borne measurements is

provided by the Ultraviolet Auroral Imager (V5), which has two cameras looking at the wave length of OI (1304 Å) and the N₂ Lyman-Birge-Hopfield (LBH) bands in the region of 1400–1600 Å. Typically, an image is acquired from a single camera every 40 seconds, and in special cases, one picture may be transmitted for every spin period (20 s) of the satellite. This is a major improvement compared to previous satellites, and the dynamic behavior of auroral forms may be studied at much shorter time constants.

A summary of the capabilities of the Viking scientific instruments is given in Table 2, along with the names of the principal investigators for each.

## The Viking Ground Station

The ground station of Viking is located at Esrange, close to the northern border of Sweden (as shown in the cover). Since the spacecraft carries no tape recorder, observations are acquired only when it is in view of the tracking station. Measurements can be made continuously from the time when Viking comes close to the auroral field lines (when it is above the polar region) until the time when it leaves the auroral field lines on the other side of the pole.

A central computer system in the Esrange station produces raw data tapes, data summary files, and quick look plots. A scientific center is in place at the ground station at which

experimenters have their own computer equipment for rapid data reduction, testing, and preliminary analysis. Special Viking campaigns are scheduled and conducted to speed up the data analysis and to encourage the interactions among the participating scientific groups. The scientific themes of the campaigns have been planned on the basis of the region of geospace sampled by Viking and the possibilities of making coordinated measurements with ground-based, balloon, rocket, and other satellite programs. During the campaigns the principal scientists and the ground-based community are represented at Esrange. This allows opportunities for discussion of the appropriate satellite modes and for exchanging ideas about the data immediately after they have been received.

## Early Viking Data

Figure 2 shows an example of the first page of a Viking quick look plot (QLP). This shows electric and magnetic field data acquired by Viking on March 25, 1986, just over a month after launch. This plot was prepared within a few hours of the data acquisition. In the upper left-hand corner is a polar invariant latitude/magnetic local time plot of a statistical field-aligned current distribution [*Iijima and Potemra*, 1976] with Viking's footprint and tick marks corresponding to the scale across the bottom. Shown on the horizontal scale are universal time, magnetic local time (MLT), invariant latitude (INV. LAT), L

value, altitude in kilometers, subspacecraft position latitude and longitude (SSP LAT and SSP LONG) in geographic degrees, and the geographic latitude and longitude position of the geomagnetic field line projected from Viking's position to a 100-km altitude, determined by using the IGRF80 model [IAGA Division I Working Group I, 1981].

The first three panels in Figure 2 provide space for the three components of the measured electric field, the fourth panel is for the peak-to-peak value during a 1.2-s interval, and the fifth panel shows the negative spacecraft potential with respect to the average of two electric field probes. The bottom three panels show the measured magnetic field, transformed from the spinning spacecraft reference frame into the geographic south, east, and radial components (labelled BSOUTH, BEAST, and BRADIAL).

The complete electric field vector was not measured during the orbit that is shown in Figure 2 because one probe pair on the spacecraft was used by the Low-Frequency Wave Experiment (V4L) for measurement of electron density fluctuations. Therefore the three electric field components are not plotted in the appropriate spaces in the QLP shown in Figure 2 (i.e., the first three panels). However, the spacecraft potential was measured and is plotted in the fourth panel. This is the negative spacecraft potential measured with respect to the average of two electric field probes. It is a measure of the electron density multiplied by the square root of the temperature. This potential fluctuates rapidly during both crossings of the auroral oval, especially near the northern edge ~75° invariant latitude on the evening side and between 70° and 80° in the prenoon sector.

The east-west component of the magnetic field (BEAST) is the most appropriate to detect perturbations associated with large-scale Birkeland currents. A large-scale magnetic perturbation can be seen in the left side of the BEAST trace near 21:00 MLT and extending from about 63° to 75° invariant latitude. This disturbance is about 150 nT and is related to the large-scale Birkeland current systems in the evening sector. A complicated set of magnetic perturbations occurs on the dayside near 08:40 MLT between ~76° and 75° invariant latitude. These perturbations are associated with the large-scale Birkeland current systems in this sector. These observations were acquired near Viking apogee, where the b⋯ ⋯mpling rate of the Magnetic Field F ⋯ ,53 Hz) combined with the low r⋯ ⋯ satellite (3.3 km/s) translates to a s⋯ resolution of 60 m. A 60-m horizontal distance at Viking's apogee altitude of about 2 $R_E$ projects along geomagnetic field lines to a horizontal distance of about 12 m near the earth's surface.

An additional three pages, displaying data acquired by the energetic particle, plasma wave, and imaging experiment, are included in the set of QLPs that are presently being distributed for a small charge to the international community of scientists. Requests for these QLPs should be addressed to the Kiruna Geophysical Institute, Kiruna, Sweden.

Figure 3 shows an energy-time spectrogram plot of ion and electron fluxes measured by the Hot Plasma Experiment (V3) during orbit 176 (shown in Figure 2). Energy in thousands of electron volts (keV) is plotted on the vertical scale, and universal time, alti-

## TABLE 2. Viking Scientific Instruments

| Experiment | Ranges | Resolution | Principal Investigator |
|---|---|---|---|
| V1 Electric Field | 0–0.5 V/m | 0.1 mV/m; (53 or 106 samples/s) | L. Block, Royal Institute of Technology, Stockholm |
| V2 Magnetic Field | ±1,024 nT ±4,096 nT ±16,384 nT ±65,536 nT | ±0.125 nT ±0.5 nT ±2 nT ±8 nT (53 samples/s) | T. A. Potemra and L. J. Zanetti, Applied Physics Laboratory, Johns Hopkins University, Laurel, Md. |
| V3 Hot Plasma Electron Spectrometer | 10 eV–300 keV | 16–128 energy steps; ΔE/E = 0.5–0.25 | R. Lundin, Kiruna Geophysical Institute, Kiruna, Sweden |
| Positive Ion Spectrometer | 1 eV–40 keV | 16–64 steps; ΔE/E = 0.05–0.10 | |
| Ion Composition (Low Energy) | 1 eV–70 keV/g | 8–32 steps; ΔE/E = 0.03–0.06 | |
| Ion Composition (High Energy) | 10 eV/g–10 MeV/g | 16–64 steps; ΔE/E = 0.07–0.25 | |
| V4L Low Frequency Waves | 0–15 kHz | | G. Gustafsson, Uppsala Ionospheric Observatory, Uppsala, Sweden |
| Plasma Density | 1–3000 cm⁻³ | | |
| V4H High Frequency Waves | 10 kHz–512 kHz | | A. Bahnsen, Danish Space Research Institute, Lyngby |
| V5 Ultraviolet Auroral Imager | 1250–1400 Å 1345–1900 Å (one image every 20–80 s) | <50 km | C. D. Anger, University of Calgary, Calgary, Canada |

## TABLE 3. The Viking Science Team

| Researcher(s) | Affiliation |
|---|---|
| Kerstin Fredga | Swedish Board for Space Activities, Solna, Sweden |
| L. Björn | Swedish Space Corporation, Solna, Sweden |
| **V1 Electric Field Experiment** | |
| L. Block, C.-G. Fälthammar, P.-A. Lindquist, and G. Markland | Department of Plasma Physics, Royal Institute of Technology, Stockholm, Sweden |
| F. Mozer | University of California, Berkeley |
| A. Pedersen | Space Science Department, ESA-ESTEC, Noordwijk, The Netherlands |
| **V2 Magnetic Field Experiment** | |
| T. A. Potemra, L. J. Zanetti, P. F. Bythrow, and R. E. Erlandson | Applied Physics Laboratory, Johns Hopkins University, Laurel, Md. |
| M. Acuna | NASA/Goddard Space Flight Center, Greenbelt, Md. |
| R. Boström and G. Gustafsson | Uppsala Ionospheric Observatory, Uppsala, Sweden |
| M. Sugiura | Geophysical Institute, Kyoto University, Kyoto, Japan |
| **V3 Hot Plasma Experiment** | |
| R. Lundin, B. Hultqvist, L. Eliasson, and I. Sandahl | Kiruna Geophysical Institute, Kiruna, Sweden |
| F. Soraas | University of Bergen, Bergen, Norway |
| W. Studemann, B. Wilken, and A. Korth | Max Planck Institute, Lindau, Federal Republic of Germany |
| J. B. Blake and J. Fennel | The Aerospace Corporation, Los Angeles, Calif. |
| D. Bryant | Rutherford and Appleton Laboratory, Chilton, U.K. |
| T. Fritz | NOAA Space Environment Laboratory, Boulder, Colo. |
| D. J. Williams | Applied Physics Laboratory, Johns Hopkins University, Laurel, Md. |
| J. B. Reagan and R. D. Sharp | Lockheed, Palo Alto, Calif. |

*(cont. next page )*

D-4

TABLE 3. (cont. )

| Researcher(s) | Affiliation |
|---|---|
| *V4H  High-Frequency Waves* | |
| A. Bahnsen, M. Jespersen, and E. Ungstrup | Danish Space Research Institute, Lyngby |
| R. Pottelette | Centre de Recherche en Physique de l'Environnement (CRPE), Saint Maur, France |
| R. Bostrom and B. Holback | Uppsala Ionospheric Observatory, Uppsala, Sweden |
| R. Gendrin | CRPE/Centre National d'Etudes des Télécommunications, Paris |
| *V4L  Low-Frequency Waves* | |
| G. Gustafsson, B. Holback, R. Bostrom, G. Holmgren, and H. Koskinen | Uppsala Ionospheric Observatory, Uppsala, Sweden |
| A. Bahnsen, M. Jespersen, and E. Ungstrup | Danish Space Research Institute, Lyngby |
| M. C. Kelley and P. M. Kintner | Cornell University, Ithaca, N.Y. |
| A. Pedersen | Space Science Department, ESA-ESTEC, Noordwijk, The Netherlands |
| *V5  Ultraviolet Auroral Imager* | |
| C. D. Anger | Department of Physics, University of Calgary, Calgary, Canada |
| A. Vallance Jones, G. Creutzberg, R. L. Gattinger, and F. R. Harris | Herzberg Institute of Astrophysics, National Research Council Canada, Ottawa |
| G. G. Shepherd and J. C. McConnell | York University, Toronto, Canada |
| A. L. Broadfoot | Earth and Space Sciences Institute, University of Southern California, Tucson, Ariz. |
| G. Gustafsson | Uppsala Ionospheric Observatory, Uppsala, Sweden |
| L. L. Cogger, J. W. Haslett, J. S. Murphree, and D. Venkatesan | University of Calgary, Calgary, Canada |
| E. J. Llewellyn and D. J. McEwen | University of Saskatchewan, Saskatoon, Canada |
| E. H. Richardson | Dominion Astrophysical Observatory, National Research Council Canada, Victoria |
| G. Rostoker | University of Alberta, Edmonton, Canada |
| G. Witt | Meteorological Institute, University of Stockholm, Stockholm, Sweden |
| *Ground-Based Experiments* | |
| R. Pellinen | Finnish Meteorological Institute, Helsinki |
| H. Opgenoorth | Uppsala Ionospheric Observatory, Uppsala, Sweden |

tude, invariant latitude, and magnetic local times are given on the horizontal scale. The observed counts per readout (a measure of particle flux) are indicated by color. These data were acquired between 20:36 UT and 20:48 UT, when Viking passed over the evening auroral zone (see Figure 2). Auroral zone particles are observed until about 20:43 UT, when the polar cap is encountered. The period from about 20:38 UT to 20:43 UT is characterized by strong particle acceleration, up to 10 keV for the electrons. The absence of ion beams, with the exception of the beam flowing upward at 20:39:30 UT, indicates that most of the acceleration occurs above Viking's altitude (above 7000 km in this case).

Figure 4 is a display of the low-frequency (V4L) wave data acquired during the orbit shown in Figure 2. During this orbit the V4L

experiment used two density probes with 80 m separation. The spectrograms in the two uppermost panels of Figure 4 provide a survey plot of spectra throughout the entire orbit, except for the period between 20:50 UT and 21:00 UT, when no data was acquired by this instrument. Data from the boom parallel to the magnetic field are shown in the top panel, and data from the probe perpendicular to the magnetic field are shown in the panel below. The frequency range plotted on the vertical scale is 0–428 Hz. The spectrograms in the bottom of the figure display data during the 5-minute interval 20:37–20:42 UT (from the bottom: density from probe 1, cross coherency between the probes, and density from probe 2). The frequency range is 0 to 428 Hz in all cases. At about 20:40 UT, both probes measured strong tur-

bulence. The white bands in the middle panel indicate high coherency between the probes. The "harmonic" structures at about 20:37 UT, 20:39:30 UT, and 20:42 UT are internal interferences from the resonant sounder experiment.

Figure 5 shows the color spectrogram for the data acquired by the High-Frequency Wave Experiment (V4H). This figure shows the electric and magnetic components in the bottom and top panels, respectively, of waves between 9 and 509 kHz (plotted on the vertical scale). This segment of data extends from approximately 20:30 UT to 20:50 UT, near the crossing of the nightside auroral zone (see Figure 2). The main feature is the development of an AKR event near 20:40 UT, and several distinct bursts of auroral hiss are also evident.

Figure 6 shows an auroral image acquired by the Ultraviolet Auroral Imager Experiment (V5) at approximately 20:47 UT during the same orbit discussed in all of the previous figures. This is a reproduction of the image received and processed in the Esrange tracking station on a nearly real-time basis. A computed outline of Greenland and Iceland are also shown in Figure 6. This image shows the presence of a form over the southern tip of Greenland (the bottom is close to midnight) that may be interpreted as a western-traveling surge (WTS).

These data from Viking's complement of scientific experiments are presented here to provide an indication of the capabilities of this program. A more detailed analysis of the space plasma phenomena is presently underway and will be presented in the future.

## Summary

The launch of Sweden's first satellite, Viking, must be regarded a major success by any measure. The real-time "campaign" mode of satellite control and data acquisition, the unique orbit, and the unrestricted and quick distribution of summary data to the international community of scientists make the Viking program unique. This program is expected to make significant contributions to the understanding of solar-terrestrial physics and space plasmas. These contributions will help provide the background and set the stage for the International Solar Terrestrial Physics (ISTP) Program, scheduled for the last decade of this century.

## Acknowledgments

# APPENDIX E

.

## Initial Report Distribution

R. Gracen Joiner                                    1 Copy
Office of Naval Research
Code 1114SP


Director, Naval Research Laboratory                 1 Copy
Code 2627


Defense Technical Information Center                12 Copies


NAVPRO/LMSC                                          1 Copy